Alma Mater Studiorum – Università di Bologna

DOTTORATO DI RICERCA IN

Chimica

Ciclo XXVII

Settore Concorsuale di afferenza: 03/D1

Settore Scientifico disciplinare: CHIM/08

SILK FIBROIN: A BIOPOLYMER PLATFORM FOR INNOVATIVE PHARMACEUTICAL FORMULATION AND BIOMEDICAL DEVICES.

Presentata da: dott.ssa Anna Sagnella

Coordinatore Dottorato   **Relatore e co-relatore**

Prof. Aldo Roda   **Prof. Carlo Bertucci**
                                                    Dott.ssa Valentina Benfenati

Esame finale anno 2015

1

Table of Contents

1. Introduction

1.1 Biomaterials

The American National Institute of Health defined and described biomaterials as "any substance or combination of substances, other than drugs, synthetic or natural in origin, which can be used for any period of time, which augments or replaces partially or totally any tissue, organ or function of the body, in order to maintain or improve the quality of life of the individual".[1]

Biomaterials of natural and synthetic origin are used in biomedicine and in tissue engineering in order to fabricate medical devices as implants, porous scaffolds, membranes and carriers for bioactive molecules. Biomaterials-based medical devices promote the replacement and the functional restoration to tissues or constituents into a living body that was deteriorated due to a disease, trauma or aging.[2] The most important applications of biomaterials in various medical devices are summarized in table 1. Accordingly, the fundamental features of biomaterials intended for medical devices can be summarized as: non-immunogenicity, biocompatibility, biofunctionality, controllable biodegradability, structural integrity and mechanical flexibility.[1-3] Some biomaterials can also be resorbable by incorporation into surrounding tissue. Biomaterials can be described and classified depending on their properties, clinical application and basic structure. Four categories of biomaterials have been identified based on structure, bonding and inherent features: **ceramics, metals, polymers and composites**.[2,3] Pure **metals** and alloys are inert materials selected exclusively to fabricate load-bearing implants (pins, screws, plates, prostheses) due to their excellent electrical and thermal conductivity, mechanical strength, corrosion resistance and reasonable costs. **Ceramics** are polycrystalline materials characterized by hardness, brittleness, mechanical strength, stiffness, low density, corrosion resistance. Although ceramics find large application in dentistry, orthopedics and as medical sensors, these biomaterials are less used in respect to metals and polymers due to plastic deformation and sensitivity to cracks and other defects.

Polymers are the best studied biomaterials in biomedical science and their application in medical devices was developed through an evolutionary process. The advantage of using polymers is mainly easy manufacturing of raw material into products of the desired shape. Polymers have unique features such as good biocompatibility, mechanical flexibility and strength, lightweight, several chemical compositions with different chemo-physical properties.

In the last decades, the need to improve chemo-physical and mechanical properties of biomaterials led to the development of processing and fabrication of **biocomposite** materials, that are generated

by adding metals and/or ceramics, as filler or reinforcement, into a polymeric matrix and/or in polymeric fibres. **Biocomposite** materials applied in biomedicine are targeted mainly for drug/gene delivery, tissue engineering and cosmetic orthodontics. Biocomposite materials are innovative and multifunctional materials and display better properties than single components.[2]

APPLICATION	MEDICAL DEVICES	BIOMATERIALS		
		METALS	CERAMICS	POLYMERS
CARDIOVASCULAR	Balloons Catheters Grafts Heart valves	Steels	Pyrolytic carbon	Nylon/Polyesther LLDPE/HDPE e-PTFE
ORTHOPEDICS	Bone screws Fracture fixation Knee bearing Hip implants Intervertebral disc Fixation Hip stem Bearings Bone grafts Bone substitutes Joint replacements Spinal implants Spinal fusion Bone cement Tendon ligament	Steels CoCr **Alloys**	Silica glass Alumina,Zirconia Coral	UHMWPE Polyurethanes PEEK PMMA/PS HDPE, e-PTFE
SOFT TISSUES	Sutures Sutures anchors Breast implants Coatings for tissue ingrowth		Carbonated hydroxyapatite	Polyester/PLLA/PGA PLDLA/PLA Silicone
DENTAL	Implants Periodontal Maxillofacial prosthetics Crown filling Cements	Titanium,Alloys	Silica glass " Zirconia,Alumina	Acrylic resins PMMA

Table 1. Main applications of biomaterials in medical devices.[2]

1.2 Polymeric Biomaterials

Currently, new strategies of processing are investigated and required in order to fabricate new medical devices and innovative matrices for drug delivery in specific sites whitin the body.[4] Among different classes of biomaterials, utilization of polymers has greatly impacted the advancement of modern biomedicine thanks to two relevant features: 1) non-toxicity of their degradation products that can be eliminated from the body via natural metabolic pathways;[5-7] 2) several opportunities to chemically and structurally modify polymers,[8-10] with the aim to improve their thermal stability, solubility, biodegradability and mechanical behaviour.

The wide range of biomedical field application includes the use of polymers as excipients in cosmetic and pharmaceutical formulations,[11,12] as well advanced biomedical device for innovative diagnostic and therapeutic applications.[13-15] Polymers are classified based on their natural (biopolymers) or synthetic origin. The main origin of synthetic polymers are the non-renewable petroleum resources; whereas, biopolymers are produced from renewable resources (animals, plants). Several naturally derived polymers offer many advantages compared with synthetic polymers: excellent biocompatibility, biological activity considering that most of them are present in tissues of living organisms, easy manufacturing that can be exploited to generate biocomposite materials, optimal biodegradability due to the action of enzymes into living organisms. Biopolymers used as biomaterials are biological macromolecules belonging to classes of polysaccharides and proteins.

1.2.1 Polysaccharide biopolymers

Polysaccharide biopolymers used in biomedical applications are classified based on their animal and vegetable origin. The most commonly used and developed are chitosan, cellulose, starch and alginate. **Chitosan** is derived from a partial alkaline N-deacetylation process of the **chitin** which is another polymeric polysaccharide used as biomaterial[16,17] and extracted from the shells of crabs, shrimp, crawfish and insects. The degree (30-100% depending on the kind of preparation) of deacetylation of chitin determines the ratio of glucosamine that affects crystallinity, surface energy and enzymatic degradation rate of polymeric chains into chitosan. The rigid and compact crystalline structure of chitosan is sustained through strong intra- and intermolecular hydrogen bonding that makes it soluble only in few dilute acid solutions. Many derivatives, largely employed in biomedical fields,[18] are produced by chemical modification of the fundamental skeleton of chitin and chitosan. **Starch** is a polysaccharide from vegetal sources extracted from potatoes, corn, wheat and rice. The structure of starch is composed of amylose, a linear and crystalline polymer, and

amylopectine, a branched and amorphous polymer with different ratios depending on the vegetable source. Biodegradability and mechanical behaviour are due to different amounts of amylose and amylopectine,[19] specifically the major amylose content increases the elongation and strength.[20] Enzymatic degradation of starch is achieved from amylases and glucosidases that attack α-1,4 and α-1,6 links, respectively. Starch-based composites, known as thermoplastic starch, are used as substitutes for synthetic polymers.[21] The water insolubility, brittleness and mechanical flexibility of starch can be improved by using two different approaches: 1) chemical modification by acetylation[22] that produces **starch acetate**; 2) by blending starch with synthetic biodegradable polymers.[23,24] **Cellulose** is another polysaccharide produced by plants and composed of linear and very long macromolecular chains of one repeating unit of cellobiose. The crystalline composition cellulose is infusible and insoluble in all organic solvents.[25] Cellulose is degraded via enzymatic oxidation with peroxidase secreted by fungi or bacteria.

Cellulose has to be chemically modified for processing. The most important derivatives of cellulose, produced following the functionalization of hydroxyl groups, are ethers, esters and acetals. Different degrees of substitution influence mechanical properties and biodegradation of cellulose derivatives.[26,27] **Alginic acid or alginate** is a polysaccharide extracted from brown algae. Alginate is a non-branched, binary copolymer composed of β-D-mannuronic acid monomer linked to α-L-guluronic acid monomer, through a 1,4-glycoside linkage in different ratios depending on different sources. Alginic acid is capable to form gels in the presence of counterions as divalent cations, such as Ca^{2+}. This feature permits the encapsulation of various components such as drugs and growth factors. These alginate-based hydrogels can be employed as scaffolds for tissue engineering, as delivery vehicles for drugs and as model extracellular matrices for basic biological studies.[28] **Hyaluronan** is a linear polysaccharide widely present in several animal species. Hyaluronan polysaccharide polymer has a very high molecular weight; it is formed by repetitive units of disaccharide constituted of N-acetylclucosamine and β-glucuronic acid and exhibits a stereochemical structure characterized by an asymmetric distribution of hydrophobic and hydrophilic chains. Hyaluronan is distributed in many tissues of the animal body, in particular in the skin, the umbilical cord and the semen, where it carries out important chemo-physical and mechanical functions due to its capacity to retain water.[29] Biodegradation of hyaluronan occurs by enzymatic reactions of endoglycosidases called hyaluronidases present in different tissues and cells. Products, such as oligo and polysaccharides, resulting from biodegradation of hyaluronan, are not toxic and have many relevant biological properties.[30] Hyaluronan, thanks to its high hydration

capacity and viscoelasticity, is used as biomaterial in order to fabricate medical devices and drug delivery systems for applications in ophthalmology, articular pathologies and esthetical medicine.[31]

1.2.2 Proteins biopolymers

Proteins show a large versatility for biomedical applications[6] for their chemical composition, that is suitable to be functionalized and structurally modified in order to have specific functional properties. Of note, many proteins that are capable of forming films, following a casting process of solution, display in some case a mechanical behaviour comparable to those of films produced by synthetic polymers. Recently, the fabrication of biodegradable and multifunctional protein-protein structural composites is emerging in biomedical science with the aim of finding innovative functional properties to improve *in vivo* and *in vitro* studies targeted to explain the impact of biomaterials on cell and tissue functions.[32] **Human serum albumin (HAS)** is the most abundant protein in blood plasma (ca. 60% of the total protein). HAS is a helicoidal protein (66.5 kDa) constituted of 585 aminoacids assembled into domains (I, II, and III) characterized by similar structures and each is formed by two subdomains (A and B). HAS can exist in two protein conformations depending on whether it is assembled with fatty acids.[33] The main functions of HAS in the body are the regulation of colloid osmotic pressure, the binding and transport of molecules which conduct antioxidant and anti-inflammatory actions in the organism.[34]Application of HSA in biomedicine is especially intended to realize drug carriers and drug delivery systems thanks to its capacity to interact and encapsulate a variety of bioactive molecules, in particular insoluble ligands such as fatty acids and porphyrins.[35,36] The nature of interaction between HAS and biomolecules or drugs influences their pharmacokinetics and pharmacodynamics. The ability of HAS to bind porphyrins has recently allowed, recently, to employ this protein for photodynamic therapy and potential oxygen carrier.[37]

Collagen is a fibrous protein from animal sources and it represents the major component of connective tissues of skin and bones. Polypeptide chains of collagen protein are composed mostly of glycine, proline, hydroxyproline and lysine aminoacidic residues. As consequence of different self-assembling and combinations between polypeptide chains, twenty-nine different types of collagen are formed and currently characterized.[38] The optimal standard type of collagen, mostly used for tissue regeneration, is type I collagen that can be extracted from various animal sources including bovine skin and tendons, porcine skin and rat tail.[39,40] Collagen is denatured and/or chemo-physically degraded in order to produce gelatine. **Gelatine** is a water-soluble protein with high molecular weight composed of 19 aminoacids. Gelatine water-solution is processed in films

characterized by mechanical and barrier properties correlated to amino acidic composition. Physical, mechanical and water vapour barrier properties of films are improved by adding gelatine solution to a variety of biopolymers as soy protein, oils, fatty acids and certain polysaccharides.[41,42] Collagen and gelatine are degraded by proteases through hydrolysis of the amide function.[6] **Keratins** are fibrous proteins produced in epithelial cells in higher vertebrates and in humans. Keratin filaments form the cytoskeleton and their functions are mechanical and protective, indeed they are particularly abundant in epithelia exposed to considerable mechanical stress such as keratinized epidermis and corneous layer of skin. Keratins proteins show chemical, mechanical and thermal stability, low sensitivity towards attacking of common proteolytic enzymes thanks to high concentration of intermolecular and intramolecular disulfide bonds formed by oxidation of amino acid cysteine residues.[43] Keratins are classified in *soft* and *hard* based on their amino acid composition, secondary structures and function. Feather and wool waste are the largest source of keratins destined for use in both industrial environment and in biomaterials research. Over the past three decades keratins proteins have been considered in the development of biomaterials used in biomedicine for drug delivery and tissue engineering.[44]

Silk fibroins (SF) are natural proteins produced from different species of arthropods, such as spiders, scorpions, silkworms, mites and bees.[45] Silks are synthesized into insect's glands and produced as fibre or filaments through a spinning process. Silkworm silks are more commercially produced and largely employed in textile industries than spider silks for following reasons: a) the higher yield of fibre that is 600–1500 m from a single silk cocoon, while only ~137 m and ~12 m from the ampullate gland of a spider and spider web, respectively; b) better mechanical properties (strength, elasticity and flexibility), c) silkworm fibres show excellent biocompatibility and biodegradability and are FDA-approved, indeed they are used for decades as suture in surgery.[45-47] Recently, the knowledge and development of innovative chemical water-based extraction and purification processes[46] promoted biomedical application of silkworm fibroin enable to process in various others formats, such as hydrogels, porous scaffolds, micro-nanoparticles.[45]

1.3 Silkworm silk fibroin from *Bombyx mori*

Silk fibroin based biomaterials are commonly fabricated from proteins of the domesticated silkworm *Bombyx mori (B. mori)* (figure 1A) that is the largest producer of silk fibres. At the end of larval stages, silkworm generates silk fibre in the form of cocoon (figure 1B) following a spinning process. The amount of fibre in a single cocoon is 600-1500 m.[47] The fibre of the cocoon consists of two protein components, fibroin and sericin (figure 1B), originally synthesized in silkworm

posterior and middle glands, respectively.[48] Fibroin is the major component of the cocoon and forms the filament core; the sericin, a water-soluble protein, cements the fibroin fibres like a glue into a cocoon.

Silk fibroin (figure 1C) is essentially a fibrous and structural protein, characterized by long-range ordered molecular secondary structures formed by a heavy (H) and a light (L) chain connected through disulfide linkages at C terminus;[49] the amino acid composition of fibroin chains is made by 12 repetitive domains in the form of clustered oligopeptides Gly-Ala-Gly-Ala-Gly-Ser, [Gly-Ala]n-Gly-Tyr, and [Gly-Val]n-Gly-Ala (n), separated by 11 amorphous regions composed of Gly-Ala-Gly-Ser and Gly-Ala-Gly-Ala-Gly-Ser. The H chain, more rich of hydrophobic amino acid residues, has a high molecular weight ($\approx$ 350 kDa) and is a essentially amphiphilic alternating copolymer block with amorphous regions. The L chain (MW$\approx$ 26 kDa) is more hydrophilic characterized by higher contents of Glu and Asp residues. The structural hierarchy of hydrophobic and copolymer blocks in *B. mori* SF displays unique self-assembly capability enabling to obtain substrates with exceptional chemo-physical, biological and mechanical features making silk fibroin a promising and first choice material suitable for innovative bio-technological applications.[50]
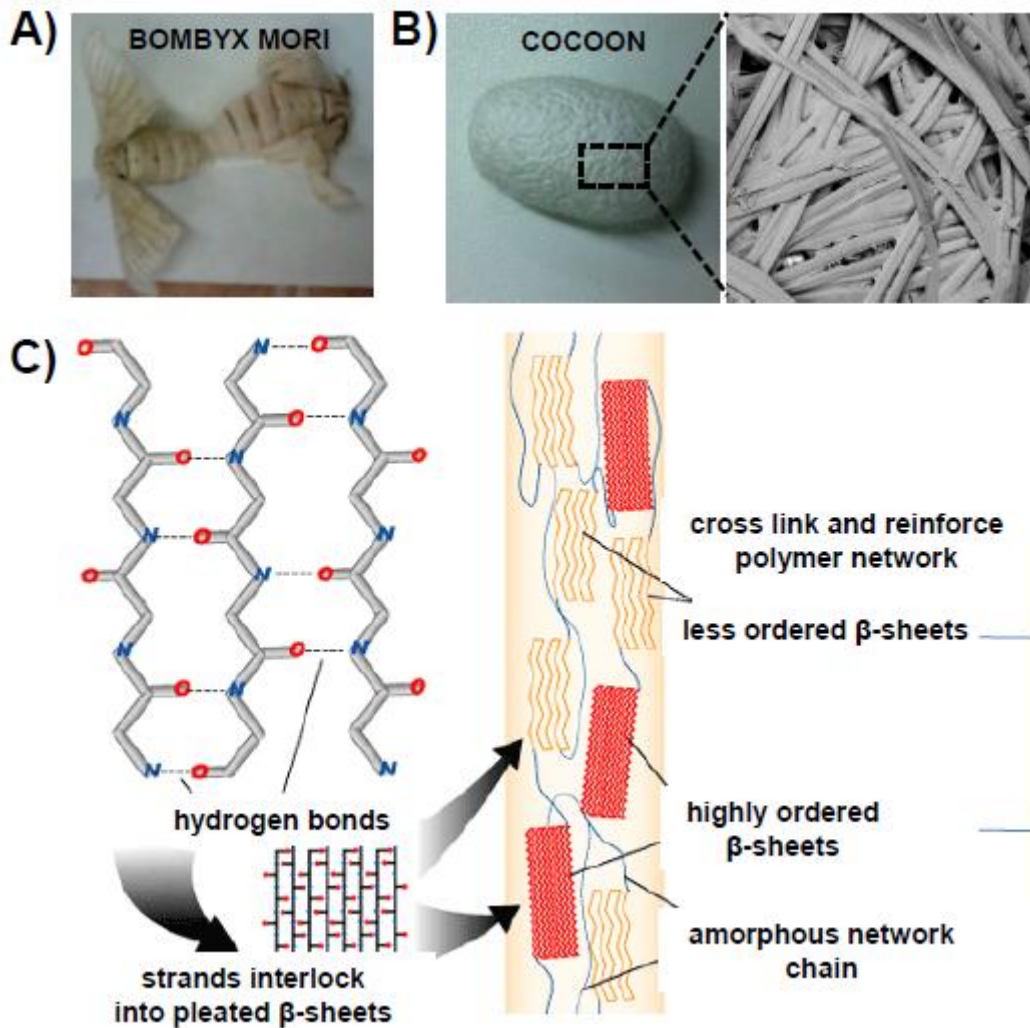
Figure 1. A) Domesticated silkworm *Bombyx mori* (Mulberry specie). B) Composition of Bombyx cocoon: fibroin fibre core, coated with sericin layer (Image from http://allthingscensored.blogspot.it/2012/04.html). C) Scheme of fibroin structure and repetitive amino acidic sequence.

Silk gland is the organ of the silk worm where the ***Native silk fibroin*** (NSF) is synthesized, assembled and spun during the last instar larvae (figure 2). Silk gland is divided in three parts: anterior, middle and posterior (figure 2A). The biggest part is the middle that is subdivided in five portions. In the last instar larvae, the silk gland constitutes almost the total amount of the larval body weight (figure 2B).

The silk fibroin is synthesized in the silkworm posterior gland, where it is present as hydrogel-like material at a polymer concentration of ca.12 wt %. The second silk protein, sericin, is produced and accumulated in the *B. mori* middle gland. When fibroin moves into middle gland, a series of processes occurs by determining the formation of a gel-like material. Exactly, a sericin layer surrounds fibroin and protein concentration increases (ca. 26 wt %) following water-evaporation through epithelial cells. Successively, the gel-like material moves forward to the anterior gland

(figure 2A) where protein concentration becomes ca. 30 wt % causing a sol-gel transition. The latter is finally spun by the silkworm at V larval stage (figure 2B) with a spinning rate of 360-80 mm/m to generate the silk cocoon (figure 2C).[51]

Silk fibroin generated in the silkworm gland is called Native Silk Fibroin (NSF). Structural, chemo-physical, mechanical and rheological properties of NSF solution have been well characterized thanks to the development of extraction methods directly from *B. mori* glands.[48,51-53] NSF solution is employed for production of silk-based biomaterials by using eco-friendly methods.[54]

However, low extraction yield combined with laborious and time consuming procedures to obtain native silk fibroin from silkworm glands has pushed research into more effective and efficient methods to obtain silk fibroin solution.
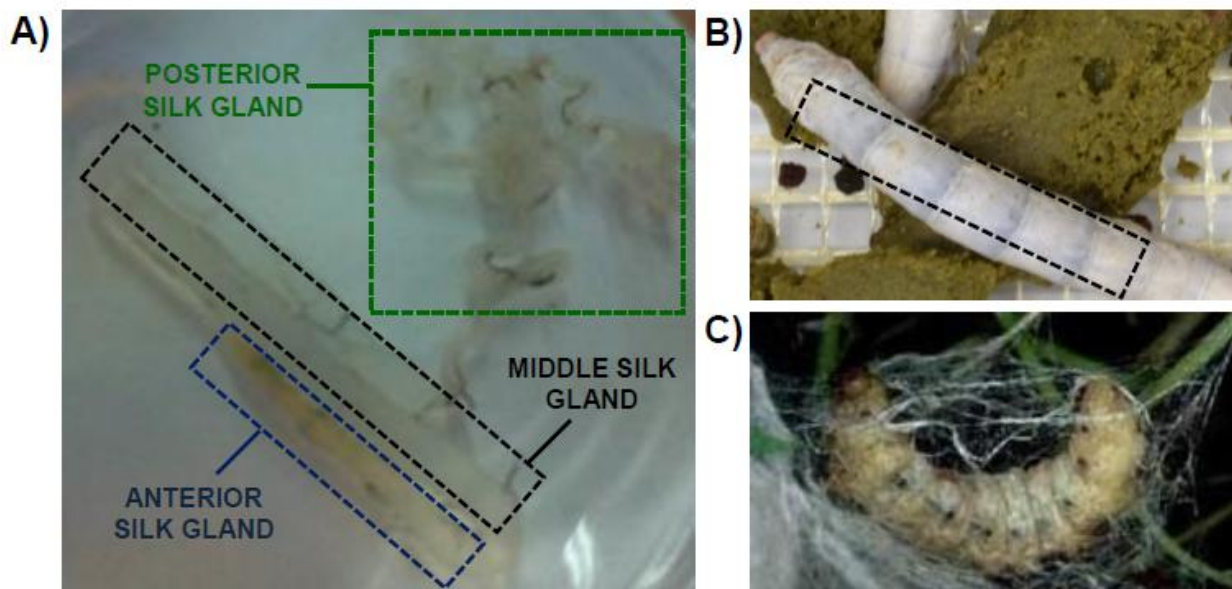
Figure 2. A) Silk gland of the silkworm *B. mori*; silk gland is divided in three parts: anterior, middle and posterior. B) Silkworm *B. mori* at V larval stage: dashed square indicates the region of the larval body occupied by silk gland. C) Silkworm insect captured during early phase of spinning to produce the silk cocoon (Image by Maryann Frazier)

In 2011, Rockwood et al. developed a completely water-based and organic solvent-free method of *reverse engineering* for extraction and purification of SF from native fibres of *B. mori* cocoons (figure 3),to obtain the so called Regenerated Silk Fibroin (RSF).[46]
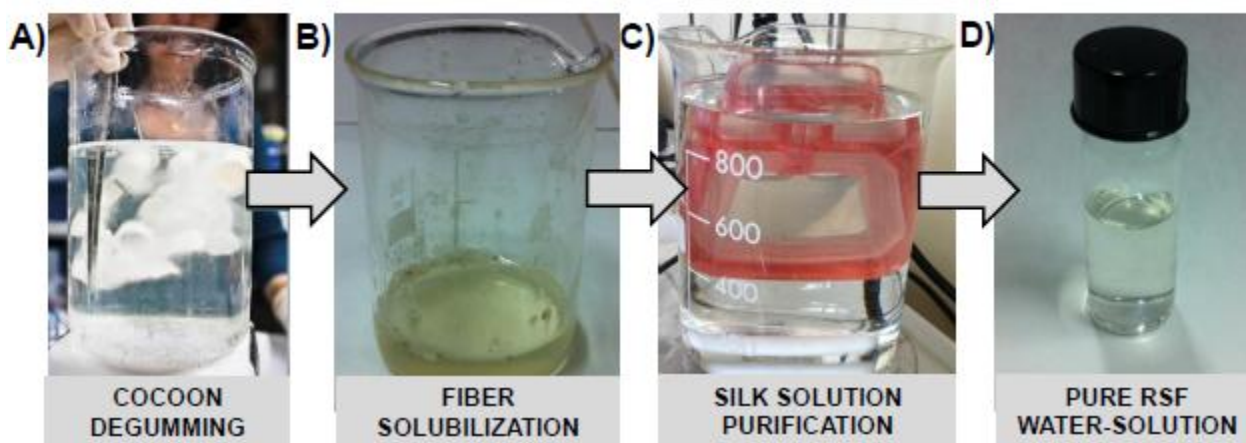
Figure 3. A-C) Main steps of extraction and purification processes of silk fibroin from cocoon: degumming in alkaline solution for removing sericin from fibres of cocoon (A), solubilisation of silk fibroin fibre in a concentrated LiBr solution (B), purification by dialysis in water of silk solution (C). D) Pure Regenerated Silk Fibroin (RSF) water-solution.

RSF water-solution is a pure protein solution with high chemical and physical stability when stored at low temperature (ca. 4°C) in order to slow down the mechanisms of sol-gel transition;[55,56] in addition RSF solution can be processed as water-insoluble films and freeze-dried powder to be stored for a long time.[57]

It is remarkable that the obtained RSF enables solution processability that is compatible with implementation in industrial environment to convert RSF solution in different formats (figure 4). Another important feature of the process is the complete elimination of the sericin component, that is known to be responsible of immunological and inflammatory response when remaining as residue in the silk fibre. In aqueous environment of RSF solution, different self-assembly mechanisms of polypeptide chains lead to the formation of defined protein structures: **a)** the crystallizable sub-domain sequence generates β-strands and 3-strand β-sheets secondary structures, extending over 20 nm, that interact with amorphous structures (random-coils and α-helix) through intramolecular interactions (hydrophobic, physical, hydrogen bonding);[58] **b)** intermolecular interactions of heavy chain form spherical micelles where hydrophobic crystallizable regions are surrounded by a shell consisting of amorphous sequences and –N and –C terminal domains.[59]

A series of conditions and external stimuli, such as fibroin concentration,[60] pH value, ion strength,[61] treatments with organic solvents, temperature,[55,56,62] shear force, mechanical stress[63] and electromagnetic field,[64] can modify the behaviour of the fibroin chains in the water-environment by determining the formation of physical intermicellar and interglobular crosslinks and an increase of β-sheets structures.[59]

When RSF water-solution is undergo to one of condition above mentioned, SF heavy chain can assume three different conformations**:** 1) **silk I**, corresponding to conformation present in the middle gland in pre-spinning, is meta-stable and water-soluble, consisting of α-helix, random-coils and β-turns secondary structures;[65] 2) **silk II,** rich in β-sheet (antiparallel and distorted) and β-turns structures, is the water-insoluble crystal form of the spun SF fibres;[66] 3) **silk III** is a 3-fold extended helix formed at air-water interface.[67]

1.3.1 RSF-based biomaterials

RSF water-solution is a versatile material that offers many possibilities for processing of SF in new material formats destined for biomedical and technological applications.[50,68,69]

The manipulation of different self-assembly phenomena of fibroin chains in aqueous environment offers control points for the development of silk-based biomaterials and/or pharmaceutical formulations. Indeed, by using a wide variety of fabrication techniques (figure 4), RSF water-solution can be converted in silk formats biomaterials such as films, hydrogels, electro-spun and wet-spun fibres, porous 3D scaffolds, micro/nanoparticles (figure 4).[70] Regenerated silk-based biomaterials display mechanical behaviour (flexibility or rigidity), chemical properties (hydrophobicity or hydrophilicity), time and ways of degradation in physiological conditions depending on different silk conformations generated during the processing of RSF water-solution.[46]

Another advantage of SF for application in biomedicine is due to its amino acid sequence that offers opportunities for chemical modification. A wide variety of chemical groups, such as amines, alcohols, phenols, carboxyl groups, and thiols have been explored as potential reactive side groups for the chemical functionalization of SF. In literature, the chemical derivatization of carboxylic acid side groups from aspartic and glutamic acids, with primary amines of peptides such as the RGD (arginylglycylaspartic acid) sequence in order to promote cell adhesion is reported.[71] Tyrosine residues also were modified with a variety of functional groups,[58,72,73] with the aim to change hydrophilicity and charge of fibroin chains and to improve the interaction of the protein with drugs.
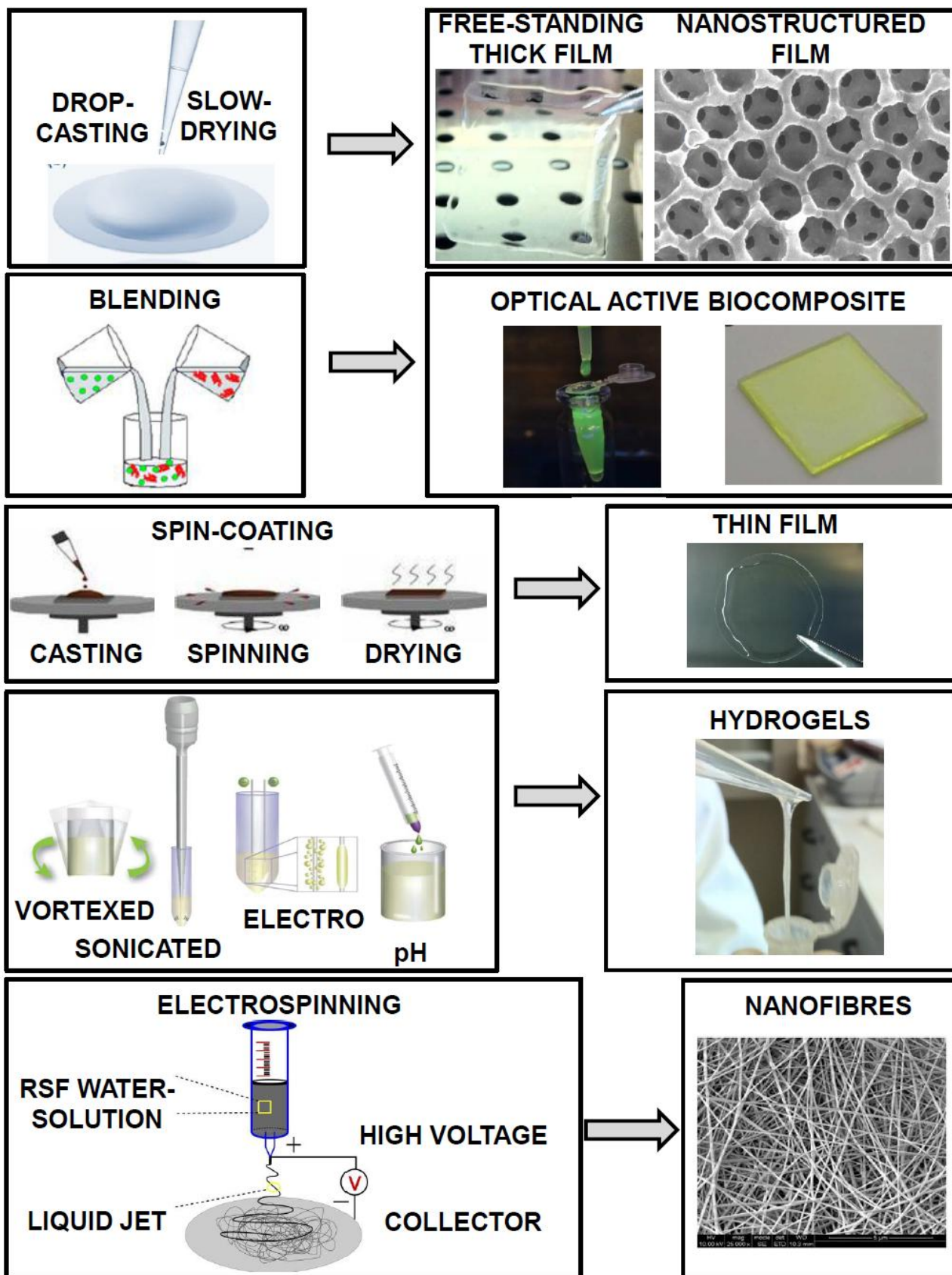
Figure 4. Scheme of different techniques used for processing of RSF water-solution and their respective products.

The applications of silk in biomedical science include four categories (table 2): 1) drug delivery systems (DDS),[50,70] 2) tissue engineering,[68,74] 3) implantable devices,[75] 4) biocompatible platforms for *in vitro* molecular/functional studies of cell cultures.[13,14]

APPLICATION	MATERIAL FORMATS	
Drug delivery system[50,70]	**Drugs/Growth factors**	
	Tablets	Adenosine, Theophylline
	Films/coatings	Penicillin, Ampicillin, Clopidogrel, Cefazolin, Indigo carmine, Genatmicin, Rifampicin, Reactive red 120, FGD2, HRP, Dextrans, BMP2, Rh-BSA, Rhodamine B, Evans Blue, Azoalbumin, Hemodin, Heparin, Paclitaxel, Clopidogrel, Adenosine
	3D-porous scaffolds	IGF1, Adenosine, Erytromycin, Rifampicin
	Hydrogels	Penicillin, Prednisone, Prednisolone, Cortisone, Hydrocortisone, Ampicillin, Buprenorphine, Benfotiamine, Trypan blue, FITC-inulin, DNA/Adenovirus,
	Injectable microcapsule/micro-nanopheres	Insuline, Salicylic acid, Propanolol Hydrochloride, Emodin, Rhodamine B
	Microneedles	Tetracycline
Tissue engineering[68,74]	**Tissue type**	
	HFIP and aqueous sponges	Bone, cartilage, soft tissue, cervical tissue
	Electrospun fibres	Bone, cartilage, vascular tissue, skin
Implantable device[75]	**Tissue type**	
	Fibers	Anterior cruciate ligament
	HFIP and aqueous sponges	Femur and mandibular defect
In vitro models[14,15,74]	**Cell Type**	
	Films	Astrocytes and DRG neurons , stem cell
	HFIP and aqueous sponges	Breast cancer and autosomal dominant polycystic kydney disease
	Hydrogels	Stem cell

Table 2. Summary of applications of different silk material formats.

2. Aim

Naturally derived polymers are traditionally defined as materials intended for biomedical science application. However, some biopolymers can substitute inorganic and plastic materials in technological devices and, at same time, modify modern manufacturing rendering it more sustainable.

To this aim, an important challenge is to identify a biopolymer capable of maintaining chemo-physical properties suitable to satisfy the requirements of current technology and appropriate to realize a convenient and cost-competitive supply chain.

In this context, SF offers several opportunities as technological material[76,77] because it is distinguished from other biopolymers thanks to relevant features, including mechanical flexibility,[78,79] optical transparency in the UV-visible range[80-81] and controllable water-solubility.[79]

Among different SF formats, film has recently found increasing applications in the electronic, optoelectronic, optic and photonic field.

In particular, recent results of the laboratories where I developed my PhD thesis and conducted research (laboratory for bio-organic interface at Institute for the Study of Nanostructured Materials, ISMN, and at Institute of Organic Synthesis and Photoreactivity, ISOF, CNR Bologna), in collaboration with the group of David Kaplan at Tufts University demonstrated and confirmed that SF film can be integrated as an efficient gate dielectric, with a high mobility value, in organic field-effect transistors (OFETs) and into organic light-emitting transistors (OLETs).[82,83] Moreover, the group showed that SF film is also very attractive for photonic applications. Toffanin et al. demonstrated that a thin-film obtained by blending RSF water-solution with Stilbene (STB) organic dye, is able of lasing action once deposited on top of an one-dimensional photonic structure.[84] Moreover, silk fibroin films are suitable substrates for adhesion and growth of primary glial cells and dorsal root ganglion neurons. Importantly by ad-hoc doping of silk films, growth factors can be delivered *in vitro* and functional properties of cultured cells can be modified and controlled.[13,14]

These important results pave the way towards the development of multifunctional silk-based optoelectronic and photonic devices, which in perspective can be made fully biocompatible or eventually bioresorbable, for innovative biomedical formulation and device for diagnostic and therapeutic purpouses. The organic solvent-free nature of the procedure and the simplified approach for device fabrication could open the view for eco-sustainable manufacturing of biomedical devices. However, to achieve this challenging goal, an adequate and controlled preparation of the core protein is required and the different steps of the value chain should be controlled. Moreover,

innovation should be promoted for processes aiming at tailoring the properties of silk fibroin substrates to fully exploit the variety and versatility of this peculiar material platform.

In this context the activity of my PhD research program can be summarized in the following objectives:

1) to define and standardize the process of extraction and purification of the RSF water-solution and production of SF films as silk-based biomaterials produced *in loco* at CNR-IBIMET (Institute of Biometeorology);[85,86]

2) fabrication and physical-chemical characterization of two-dimensional substrates (films) of fibroin;[85,86]

3) to apply different methods of manufacturing approaches with chemical and/or physical preparation of the films of fibroin;

4) to define the properties of innovative silk fibroin films nanocomposite;[79,87]

5) to study and define innovative methods of functionalization of the silk fibroin solution and films.

All the activities were developed thanks to the collaboration with a broad team of researchers and research directors of three different institutes CNR Bologna: IBIMET, ISOF and ISMN and the Laboratory of high technology Network of Emilia Romagna MIST E-R.

3. Materials and Methods

3.1 Silkworm rearing

Silkworm culture was performed in Institute IBIMET of CNR Bologna and the procedures are reported in the literature.[80,85,86] The insect breeding started from eggs belonging to the germplasm collection of the CRA-API (CRA, Honey bee and Silkworm Research Unit, Padua), which also provided an artficial diet. The strain chosen for the experiment was the polyhybrid with white oval cocoons. Silkworm were reared in plastic boxes, with different size proportional to the larvae age, placed in a Thermo stabilized (25±1°C) room with controlled relative humidity (RH > 85%) and photoperiod (12h light:12h dark).[88,89] During the whole larval stages the insects were fed ''ad libitum'' with artificial diet until the last days of the fifth instar before the spinning of the cocoons. The preparation of artificial diet was performed in order to avoid the alteration of contained nutrients as much as possible.

3.2 Extraction of Native silk fibroin

The extraction of native fibroin from silk glands was developed and performed in IBIMET by Camilla Chieco. Native silk fibroin (NSF) was extracted from the glands of 5th instar larvae before spinning; the fibroin extraction from the middle division of silk gland (MSG) was performed according to Hossain et al.[51] with a partially modified protocol, while the posterior parts of the gland (PSG) were treated according to Mandal and Kundu.[90] In brief, the entire silk glands were pulled out from the abdominal side of the worm and the middle part was separated from the posterior part. The middle glands were washed in deionized water and the surrounding epithelium was gently removed; the glands were immersed in 3 mL of distilled water to remove most of the insoluble sericin protein. After 6 h the water was removed and other 3 mL of distilled water were added and the solution was maintained at 5°C until the total dissolution of fibroin; then the solution was collected in a Falcon tube and stored in a refrigerator. The posterior glands were washed with distilled water to remove traces of sericin and placed into a beaker containing 3 mL of distilled water; the glandular tubes were cut in small pieces and gentle shaking for 1 h, then kept in refrigerator overnight. After one day, the protein released from the glandular tissues was collected in a Falcon tube and stored in a refrigerator.

3.3 Extraction of Regenerated silk fibroin

RSF water-solutions were extracted from the *B. mori* cocoons (CNR-IBIMET, Bologna) produced by silkworms fed as reported in section 3.1. The protocol for extraction and purification of silk fibroin was performed and standardized in ISOF institute of CNR Bologna according to the procedures described in literature.[46] Specifically, the cocoons were degummed in a boiling 0.02 M Na_2CO_3 (Sigma-Aldrich, St Louis, MO) solution for 45 min to obtain SF fibres that were then rinsed three times in Milli-Q water and dissolved in a 9.3 M LiBr solution at 60°C (4-6 h). The SF solutions were subsequently dialyzed (dialysis membranes, MWCO 3500) against distilled water for 48 h and centrifuged to obtain the pure regenerated SF solutions (ca. 6-8 w/v%). The RSF water-solutions were stored at 4°C.

3.4 Fabrication of SF-based biomaterials films

SF films were fabricated by different methods (figure 8) .

1) *Drop-casting and slow-drying* (DC), an exact volume of silk solution (NSF and RSF) was casted on a glass and/or polydimethylsiloxane (PDMS) support and then dried under a sterile hood at room temperature (figure 8A).

2) *Drop-casting and dried in oven* (DO): an exact volume of SF water-solution was casted on a glass or PMMA support and then dried in oven at 50°C (figure 8B).

3) *Vertical deposition* (VD): SF water-solution was deposited on glass substrate by vertical deposition in a oven at 50°C (figure 8C).

4) *MeOH treatment*: films obtained by DC approach were immersed in methanol for 1 h in order to induce protein conformation transition (figure 8D).

Preparation of hybrid silk fibroin nanocomposite films.

An organic-inorganic hybrid SF-hydrotalcites (SF-HTlc) nanocomposite (figure 13) was achieved according to the protocol published in reference 79. Briefly, RSF water-solution was mixed with a colloidal aqueous dispersion of HTlc nanoparticles (synthesis is described in the literature).[79] SF-HTlc nanocomposite films were made by using the DC approach. Specifically, films with a thickness of around 20 μm (measured by a profilometer KLA Tencor P6) were obtained by casting a drop (160 μL) of SF-HTlc water-solution on 19 mm diameter glass coverslips; while and successively drying it for 4 h in a sterile hood. Free-standing hybrid films were produced by casting various aliquots of SF-HTlc solutions on a support/mold of PDMS.

Nanostructured silk fibroin–single walled carbon nanotubes (SF-SWCNT) films were prepared according to the protocol published in reference 87. Briefly a polystyrene mono-disperse beads (PB) solution (synthesized as previously reported)[91-93] was mixed with a SWCNTs (supplied by Yangtze Nanomaterials Co, Shanghai, PRC) water-suspension in order to have blend aqueous solution (PB = 0.5 mg mL^{-1} and SWCNTs = 0.1 mg mL^{-1}); PB-SWCNTs blend solution was deposited on glass microscope slides by VD approach; **2)** 200 μL of a RSF water-solution (0.1 w/v%) were dropped on the PB-SWCNT template (formed on glass microscope slides) and **3)** dried under hood at room temperature; **4)** PB beads were removed from the SF-SWCNT bio-composite films by submerging the samples in limonene (p-mentha-1,8-diene) for 48 h used as solvent of the PB; **5)** the samples were rinsed in ethanol to quickly remove limonene adsorbed (figure 17).

3.5 Silk fibroin Biodoping

According to literature,[94,95] RhB was mixed into the artificial diet at a concentration of 0.05 wt%. Three groups of the white strain (polihybrid with oval cocoons), each composed of twenty last instar larvae were placed in a separated box and fed with the RhB-doped diet starting from the 3rd (group A), 4th (group B) and 5th (group C) day of the 5th instar until the silkworm starts spinning the cocoon. In this way, we obtained different add-eat time cocoons of 72, 48 and 24 hours, respectively. In the same manner, three groups of 5th instar larvae of the same strains were separated and fed with non-doped artificial diet and used as the control.

3.6 Silk fibroin Silylation

A hydrophobic fluorophore ester ended oligothiophene (T_3)[96] was dissolved in APTES (final conc. 0.025 M) (figure 26A-B). After sonication (15 min) this solution was added to RSF water-solution and stirred for 1 h on a tube rotator. In this way a SF-APTES-T_3 blend was formed with following concentrations: SF 4 w/v%, APTES-T_3 0.5% v/v and T_3 1.25·10^{-4} mmol. Finally, purification by size exclusion chromatography (SEC, Sephadex G25 desalting column), using DI water as eluent, was performed (figure 26C).

3.7 Chemo-physical investigations

SDS-Page. SDS-PAGE protein extraction was performed as follows: silk cocoons were fractioned into small pieces and homogenized with 100 μL of lysis buffer (50 mM TRIS-HCl, pH 7.4, 100

mM NaCl, 1 mM PMSF, 1 mM EDTA, 5 mM Iodacetamide, 1% Triton X-100, 0.5% Sodium dodecysulphate, 1% β-mercaptoethanol and Urea 8M). The extract was sonicated for 10 minutes in 20 seconds intervals every 2 minutes and pelletted for 30 minutes at 12000 rpm. The supernatant was collected and used to determine the protein content using the Bradford method. Samples were kept at 50°C or 90°C for 10 minutes and 50 µg of lysates were separated by 8-16% TGX Any-Kd gradient gel (Biorad).

Nuclear magnetic resonance (NMR) characterisation. The NMR spectra were recorded on a Varian spectrometer operating at 400 MHz (1H) and 100.5 MHz (13C). RSF solutions were first lyophilized to remove water and re-dissolved in D_2O.

Fourier Transform Infrared (FT-IR) spectroscopy. The Mid IR (400–4000 cm^{-1}) absorption measurements were carried out in a Bruker IFS-88 FT-IR interferometer at 4 cm^{-1} resolution averaging over 512 scans in order to improve the signal to noise ratio. Absorption spectra have been performed on thin silk fibroin films casted on infrared transparent substrates (KBr single crystals). The curve fitting of overlapping bands of the infrared spectra covering the amide I and II regions (1500–1700 cm^{-1}) were performed by using the Levenberg–Marquardt algorithm implemented in the OPUS 2.0 software for IFS-88 hardware control and spectral processing.

Attenuated total reflection (ATR) FT-IR spectroscopy. ATR spectra of free-standing silk films were performed by means of a FT-IR Bruker Vertex 70 interferometer equipped with a diamond crystal single reflection Platinum ATR accessory. Free-standing silk films were obtained by casting an aliquot of silk solutions on support/mold of polydimethylsiloxane (PDMS), left dried, and piled off from the PDMS substrate. The curve-fitting of overlapping bands of the infrared spectra covering the amide I and II regions (1500–1700 cm^{-1}) were performed by using the Levenberg–Marquardt algorithm implemented in the OPUS 2.0 software.

Raman spectroscopy. Raman analysis of SF-SWCNT samples was performed using a Renishaw 1000 micro-Raman system exciting at 632.8 nm (HeNe laser) and 488.0 nm (Ar + laser). The laser beam was focused through an 80x objective to a spot of approximately 1 mm. To avoid the local heating of the film in the laser spot during the analysis, the laser power density was maintained at a lower value than 10 kW cm^{-2}.

UV-VIS optical analysis. A Jasco V-550 UV-VIS spectrophotometer was used in order to obtain the UV-VIS absorption spectra from the protein solutions and the percentage transmittance from the SF films. These were prepared by casting a 40 mL aliquot of silk solution on a quartz substrate (area of 1.44 cm^2), and it was then left to dry in a sterile hood. The thickness of the films was measured by a profilometer KLA Tencor P-6 and a result of around 20 mm was obtained.

The fluorescence properties of the SF solutions and films were collected by using a Spex 1934D phosphorimeter.

Thermal analysis. The thermal properties of the silk films were measured in a DSC (Differential Scanning Calorimetry) Instrument (METTLER TOLEDO) under a dry nitrogen gas flow of 70 ml min^{-1}. The samples were heated at 2°C min^{-1} from 35 to 350°C. Thermogravimetric analyses (TGA) on different silk films, previously conditioned at 75°C of relative humidity (RH) using saturated solution of NaCl, were performed in air up to 700°C (temperature ramp of 2°C min^{-1}) by a STA1500 system equipped with a simultaneous thermal analyzer.

Silk films degradation and dissolution assay. For degradation test, silk films were incubated at 37°C in a 3 mL solution of 1 mg mL^{-1} protease XIV (Protease from Streptomyces griseus Type XIV, ≥3.5 units/mg solid, Sigma) in phosphate buffer saline (PBS) at pH 7.4. Each solution contained an approximately equivalent mass (50 ± 2 mg) of silk films (thickness ~60 μm). Solutions were replenished with enzyme and collected daily. At designated time points, groups of samples were rinsed in distilled water and prepared for mass balance. Samples were dehydrated in an oven at 50°C for 2 h. Following removal from the oven, the samples were weighed and returned to a new solution with fresh enzyme. Percent weight loss over time was determined. Each experiment was performed in triplicates. For dissolution experiment films were incubated at 37°C in a 3 mL solution of PBS at pH 7.4. The next steps follow the degradation procedure reported above.

Atomic force microscope (AFM). Atomic force microscope (AFM) topographical images were collected using an NT-MDT solver scanning probe microscope in tapping mode.

Contact angle measurement (CA). The wettability of the SF films (formed on glass substrate) was investigated by measuring the cellular medium contact angles on the silk samples by the static

sessile drop method and using a Digidrop GBX Model DS. For each film at least four drops were measured.

Mechanical tests. Stress-strain mechanical tests were carried out using a Zwick Roell Z1.0 testing machine with a 200 N static load cell. The Young's modulus (the slope of the stress−strain curve in the elastic deformation region), stress at break (the tensile stress at the breaking point of the specimen), and elongation at break (the percentage increase in length that occurs before the sample breaks) were measured on rectangle shaped film stripes, obtained using a cutting machine, length, and width of which were 50 and 5 mm, respectively. The thickness of the film stripe, determined with an uncertainty of 1 μm, was in the range of 35–40 μm. An initial grip separation of 10.000 ± 0.002 mm and a crosshead speed of 15 mm min^{-1} were used. At least four replicate film stripes were analyzed. The data were elaborated by the TestXpert V11.0 Master software. The area under the stress-strain curves was used to calculate the modulus of toughness, which is a measure of the energy that a sample can absorb before it breaks.

Scanning Electronic Microscopy (SEM). The elemental analysis of metals of SF-HTlc nanocomposite films was conducted with a scanning electron microscope (SEM, ZEISS LEO 1530 FEG) fitted with an EDS detector.

3.8 Biocompatibility studies

DRG cell culture preparation. DRG neurons from post natal p8–p18 rats (Spraugue Dawley) were dissected and dissociated by enzymatic digestion as described previously.[14] An equal amount of cell suspension was dropped onto nSF/SWCNT and nSF substrates and placed in a 37°C, 5% CO2 incubator. Cells were maintained in Dulbecco's Modified Eagles Medium (DMEM), Gibco, and 10% Fetal Bovine Serum (FBS) was added in the presence of 50 ng mL^{-1} Nerve Growth Factor (NGF), and 1.5 mg mL^{-1} cytosine b-D-arabinofuranoside, (AraC, Sigma) to reduce glial cell expression.

Primary cultures of Dorsal Root Ganglion were prepared at the Department of Human and General Physiology of University of Bologna, UNIBO. All the procedures to prepare the cultures as well as those necessary to handle the animals before and after the cell culture preparations have been performed according to the approved procedures by the Ethical Committee for Animal Experimentation of the University of Bologna.

Cell viability assay and imaging. Cell cultures were characterized after several days *in vitro* (DIV), using the fluorescein diacetate assay and optical imaging with a Nikon Eclipse Ti inverted microscope equipped with a 20x objective and CoolSNAP EZ CCD camera. Images presented are representative of 4 different cell culture preparations. Results were analyzed using one-way analysis of variance (ANOVA) or the Independent Student t-test. Data are reported as the mean ± standard error (SE) from at least three separate experiments. A statistically significant difference is reported if $p < 0.05$ or less.

4. Results and discussions

The implementation of my research program involved four major research activities whose results are in line with the objective of my PhD research program and they have been documented by 12 scientific articles published in major peer reviewed international journals (see publication list, section **6**). The most important obtained results I contributed are reported in the following four different subchapters.

4.1 Standardization of extraction and purification process of regenerated silk fibroin solution.

4.2 Fabrication and chemo-physical characterization of two-dimensional substrates (films) of fibroin.

4.3 Properties of innovative multifunctional silk fibroin films nanocomposite.

4.4 Innovative methods of functionalization of the silk fibroin solution and films: Silk fibroin Biodoping and Silylation.

4.1. Standardization of extraction and purification process of regenerated silk fibroin solution

Technology intended for biomedical applications requires adequate extraction and preparation of the core protein, control of primary and secondary structure of the extracted protein as well as a detailed control of chemo-physical and biocompatibility properties assessment of SF substrates. In this view, my first research aim was to establish *in loco* an efficient and optimal method for extraction and purification of SF from cocoon.

Different methodologies for fibroin extraction were tested and developed in the recent years. Notably, Kaplan and colleagues[46] have developed a method to produce an aqueous RSF solution, extracted from silk cocoons, avoiding the application of strong organic solvent. We follow the Kaplan's protocol and the products of every single step were monitored and analyzed to optimize and standardize the process.
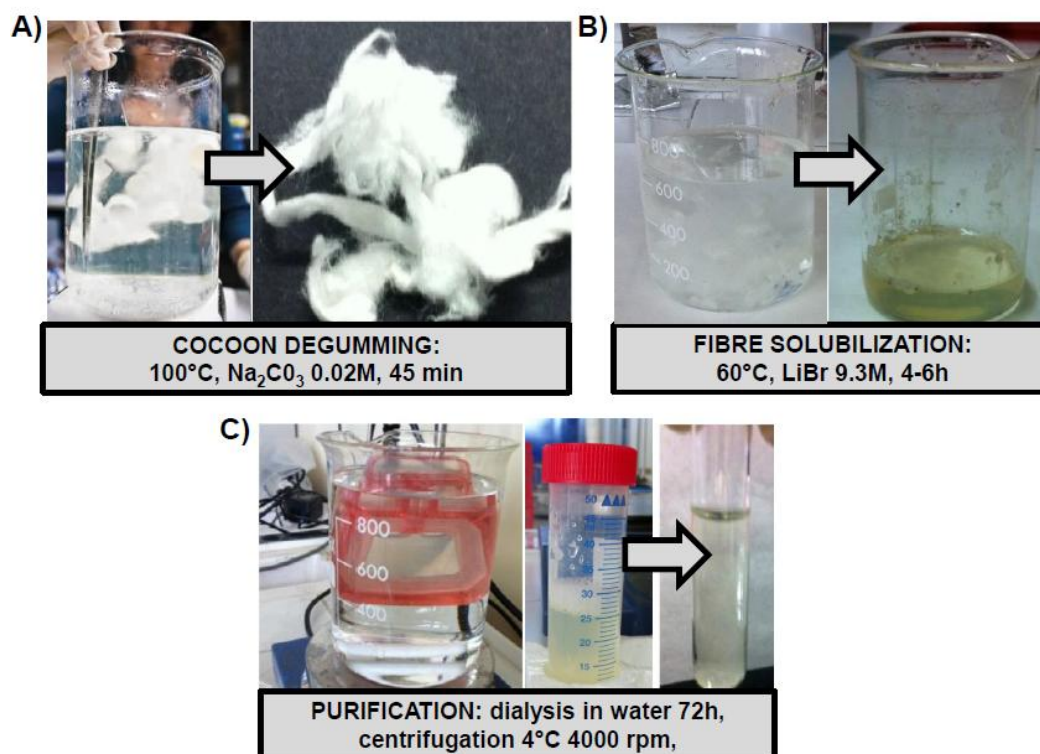
Figure 5. Illustration of the major steps of extraction and purification process with their corresponding products. A) Degumming process of silk cocoons into alkaline solution at 100°C for 45 min (left panel) and obtained fibroin fibre (right panel). B) Fibre dissolution in concentrated LiBr solution at 60°C for 4-6 h (left panel) and achieved concentrated fibroin solution (right panel). C) Purification steps: dialyses in water (left panel) and centrifugation; diluted and purified RSF water-solution (right panel).

Two output parameters were monitored during the procedure of RSF extraction and purification: the % of weight loss of the dried fibre after the degumming procedure and the concentration of the obtained RSF at the end of the extraction procedure. We found that boiling the cocoons for 45 min was the optimal time with an average loss in weight at 27.24 ± 1.56% (n = 24 extractions) which was in line with the data reported in literature.[97]

The average final concentration of regenerated fibroin in the aqueous solution was 7.13 ± 0.57 w/v% (n of extractions = 24), which is a value in line with those obtained with previously reported protocols.[46]

Since it was demonstrated that increasing the degumming time degraded silk fibroin causing the decrease of the molecular weight,[98] investigation on extracted-protein degradation as a function of the implemented extraction protocol, SDS–PAGE analysis was performed[99] on both the regenerated and native fibroin water-solutions obtained according to the protocols reported in Materials and Methods section. We observed (figure 6A) a band close to 350 kDa that is a value in good

agreement with the expected homogeneous silk fibroin composition, in particular, this protein fraction corresponds to the heavy protein chain.[99]

Amino-acidic composition of regenerated silk was explored by NMR analysis. The ^{1}H NMR spectrum of RSF in deuterated water (figure 6B), recorded at room temperature, confirmed that the samples, obtained by our procedure, are pure and the amino-acids composition we identified (Alanine (Ala), Glycine (Gly), Serine (Ser), Tyrosine (Tyr), Valine (Val) and Phenylalanine (Phe) (figure 6B) is in accordance with previous literature reports.[100,101]
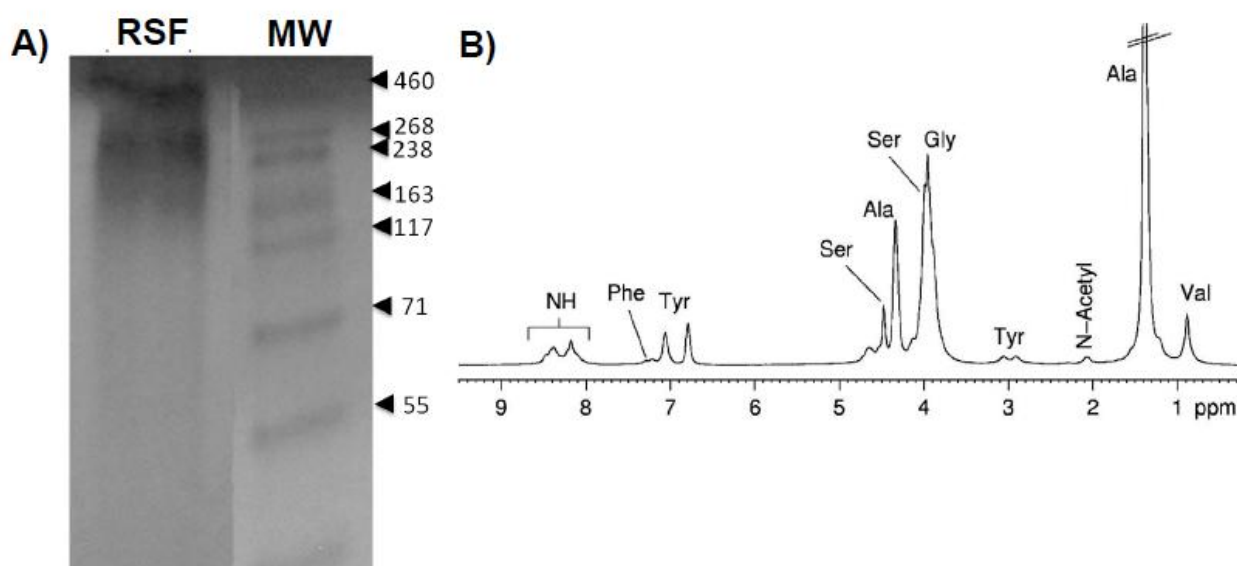
Figure 6. A) SDS-PAGE analysis of protein components in RSF water-solution dissolved in standard sample buffer. MW: molecular weight markers. B) ^{1}H NMR spectrum of RSF in deuterated water.

SF molecular conformation and protein secondary structures were investigated in the structure of silk fibroin films, prepared by DC method, through FT-IR spectroscopy in the amide regions (1200-1800 cm^{-1}).

In film obtained from RSF water-solution, in the amide I region a strong peak appears at 1655 cm^{-1} corresponding to silk I structure (figure 7A, red line). In the amide II region, peaks are observed at 1535 cm^{-1} (silk I) and at 1515 cm^{-1} (silk II), while in the amide III region, a peak appears at 1240 cm^{-1}.[102] These data indicate that the conformational structure of the protein in RSF films resembles those previously reported for films prepared with drop-casting and slow-drying method process, in which there is a dominance of the silk I structure (random coils and alpha-helices) compared to the silk II.[14]

We also explored and compared the properties of NSF solution, extracted in laboratories of IBIMET according to the method reported in Materials and Methods section. The comparative analyses of FT-IR spectra performed on NSF and RSF films (figure 7A) revealed that in NSF (figure 7A, black line), together with the bands assigned to silk I conformation, some typical peaks at 1621 cm^{-1} and 1228 cm^{-1} (β-sheet structures), generally attributed to silk II confomation[102] are observed. These results are in line with those previously reported indicating a more crystalline state of SF protein is present in NSF compared to RSF.[103]
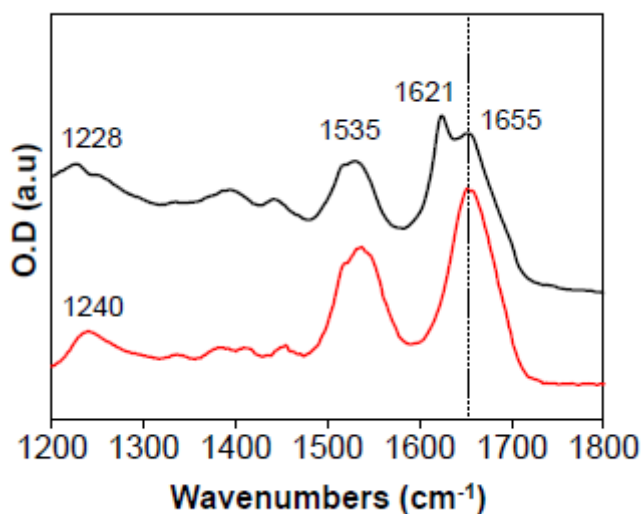
Figure 7. FT-IR spectra of NSF and RSF (black and red trace respectively).

4.2 Fabrication and chemo-physical characterization of two-dimensional substrates (films) of fibroin

Self-assembly of fibroin chains in water is a crucial point for fabrication of silk-based biomaterials intended for biomedical and technological applications. In this context, we processed RSF water-solution in films by exploring different approaches that are described in Materials and Methods section and summarized in figure 8. The chemo-physical properties of the silk films obtained by different methods are next analyzed and compared.
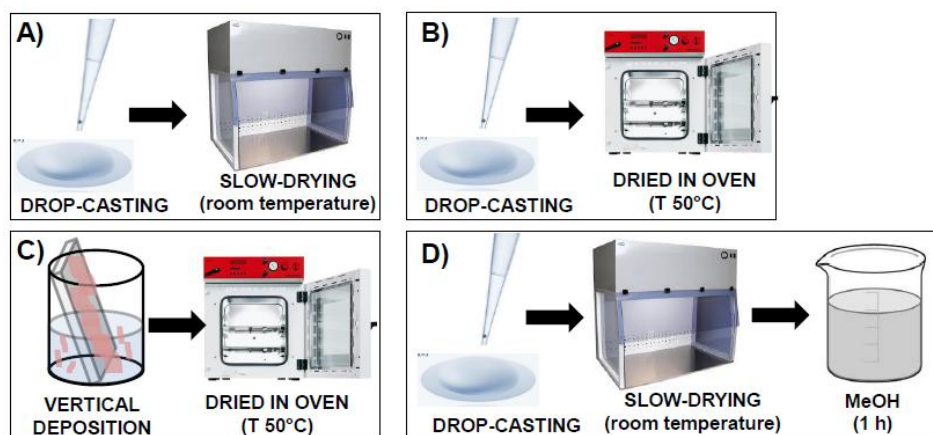
Figure 8. Scheme of different approaches employed for fabrication of SF-based biomaterials films: A) drop-casting and slow-drying (DC), B) drop-casting and dried in oven (T 50°C) (DO), C) vertical deposition in oven (T 50°C) (VD), D) drop-casting and slow-drying with treatment in MeOH (films are immersed in the organic solvent for 1 h).

Vertical Deposition is a micro-fluidic method that exploits the steady-state unidirectional convective assembling of fine particles onto a hydrophilic substrate immersed in the aqueous suspension under controlled temperature.[104] The deposition of particles on the substrate depends on the movement of particles suspended in the thin liquid film at the meniscus of the suspension.[105] It has been hypothesized that both lateral capillary force (i.e. attractive force between the particles) and the surface tension are involved in the movement of particles from the water surface to the deposit and the influence of these forces on the final fibroin structure cannot be excluded. RSF is a micellar solution,[59] we investigated the "vertical deposition" (VD) method that can be applied to deposit micelles of fibroin into two-dimensional arrays.[104,105]

As a comparison, further silk films were prepared by using different approach: 1) drop-casting and slow drying (DC) where silk solution was casted on substrates (glass and PDMS) and dried at room temperature; 2) dried in oven (DO) where protein solution was casted on substrates (glass and PDMS) and dried at same temperature of VD process; 3) treatment in MeOH, films obtained by DC method were immersed in MeOH to induce protein conformational changes.[60,62]

The effect of different self-assembly mechanisms that occurred for film formation were investigated by analysing following features of RSF in films: **a)** optical transparency recorded in UV-VIS region; **b)** protein conformational characteristics (FT-IR spectroscopy and thermal analyses, DSC and TGA); **c)** biodegradation and dissolution rate in aqueous environment (in protease solution and in DMEM cell culture medium, respectively); **d)** morphological properties (AFM); **e)** wettability and surface energy (contact angle measurements); **f)** mechanical behaviour (stress-stain test).

Silk film optical and conformational properties. UV-VIS transmission spectra of RSF films obtained with the different methods are reported in figure 9A. All the mentioned methods are able to obtain highly transparent (up to 95%) in the visible region (300-800 nm) with a clear consistent decrease under 277 nm as a result of protein absorbance. The small difference of the absorption at 277 nm for the different samples is due to the non-homogeneous thickness of the films which is strictly related to the approaches used for film fabrication. Conformational properties of fibroin processed in different films were determined by FT-IR spectroscopy and thermal analysis (DSC and TGA). As shown in figure 9B, in all types of SF films the following infrared absorptions appeared: the 1648-1654 cm^{-1} and 1535-1542 cm^{-1} regions are assigned to silk I conformation (random coil);[102,106] and the 1515 cm^{-1} band, due to C-C stretching of the aromatic ring and C-H bending of tyrosine residues in the side chains,[106] corresponding to silk II conformation. Differently, only the infrared spectra of SF-VD and SF-DC/MeOH films (figure 9B, blue and green line, respectively) displayed the typical peaks attributed to silk II conformation: at 1700 cm^{-1} (β-sheets intermolecular) and 1628 cm^{-1} (β-sheets intramolecular) in the amide I region; moreover, in the amide III beside the β-sheets band the signal for pure turn structure at 1265 cm^{-1} was observed.[106] These results indicate that drop-casting followed by water evaporation in oven at 50°C (DO method) does not change substantially the silk protein conformation; indeed, the infrared spectra of SF-DC and SF-DO films (figure 9B, black and red line, respectively) are quite similar with a slight increase of the band at 1515 cm^{-1} (silk II conformation); on the other hand, the VD process led to changes in the self-assembling of polypeptide chains in SF-VD films comparable to those observed for SF-DC/MeOH films. The presence of silk II conformation in SF films treated in MeOH is in agreement with literature data.[60,62]

In figure 9C, standard DSC curves of silk films are reported. All samples showed an endothermic peak between 50 and 100°C that can be assigned to the loss of adsorbed water. The SF-DC and SF-DO samples (figure 9C, black and red line, respectively), in contrast to the other ones, showed a non-isothermal crystallization peak at around 213°C due to the transition of unstable non-crystal structures (random coils and α-helices) to β-sheet in agreement with data reported in the literature.[107,108] After reaching the crystallization temperature, the films started to degrade with an endothermic peak at around 257°C. In the SF-DO sample this peak appears broader than in SF-DC film, indicating a probable coexistence of diverse silk crystalline structures with different degradation temperatures. Indeed, FT-IR data indicated besides the predominance of the silk I structure a slight increment of the band at 1515 cm^{-1} related to the silk II conformation (figure 9B, red line).

The endothermic peak (~ 50°C) of SF-DC/MeOH film, related to the loss of adsorbed water decreased in intensity and shifted to lower temperatures, implying that the silk film became hydrophobic absorbing a lower amount of water (figure 9C, green line). As expected, the crystallization peak disappeared because of the formation of β-sheet structures before thermal treatment; on the other hand, the degradation peak increased to 264°C, suggesting a higher thermal stability in comparison to the soluble SF-DC and SF-DO samples. For the SF-VD sample a similar thermal behaviour was observed until 250°C (figure 9C, blue line). After this temperature a relevant difference is observed: two degradation peaks appears at 266°C and 287°C. Both are higher compared to the previous ones and can be related to the stability induced by β-sheets structures. Given that the stability of the protein is related to its crystalline degree, probably the vertical deposition method induces the formation of a more stable crystalline structure of silk.

According to the FT-IR results, the crystal structure of SF-DC and SF-DO samples was mainly composed of silk I, while SF-VD and SF-DC/MeOH had a higher β-sheet content.

Given that silk I crystals degraded around 250°C and silk II (β-sheet) around 260°C, the increase of these degradation peaks for SF-VD and SF-DC/MeOH samples indicate a greater stability compared to the other films, in agreement with the dissolution and biodegradation results following reported.

Finally, TGA data of the different SF samples conditioned at relative humidity of 75% confirmed weaker water–silk interactions following the increase in silk II content (figure 9D). In fact, compared with the soluble drop casted silk film dried at room temperature (figure 9D, black line), the water content decreases from 10.9% to 10.4%, 8.8% and 7.9% for SF-DO (red line), SF-DC/MeOH (green line), and SF-VD (blue line) samples, respectively; SF-DC and SF-DO samples, characterized by a similar secondary structure (random coil and α-helix) shows a comparable weight loss, instead for the SF-DC/MeOH and SF-VD samples the water content decreases because of the predominance of β-sheet structures.
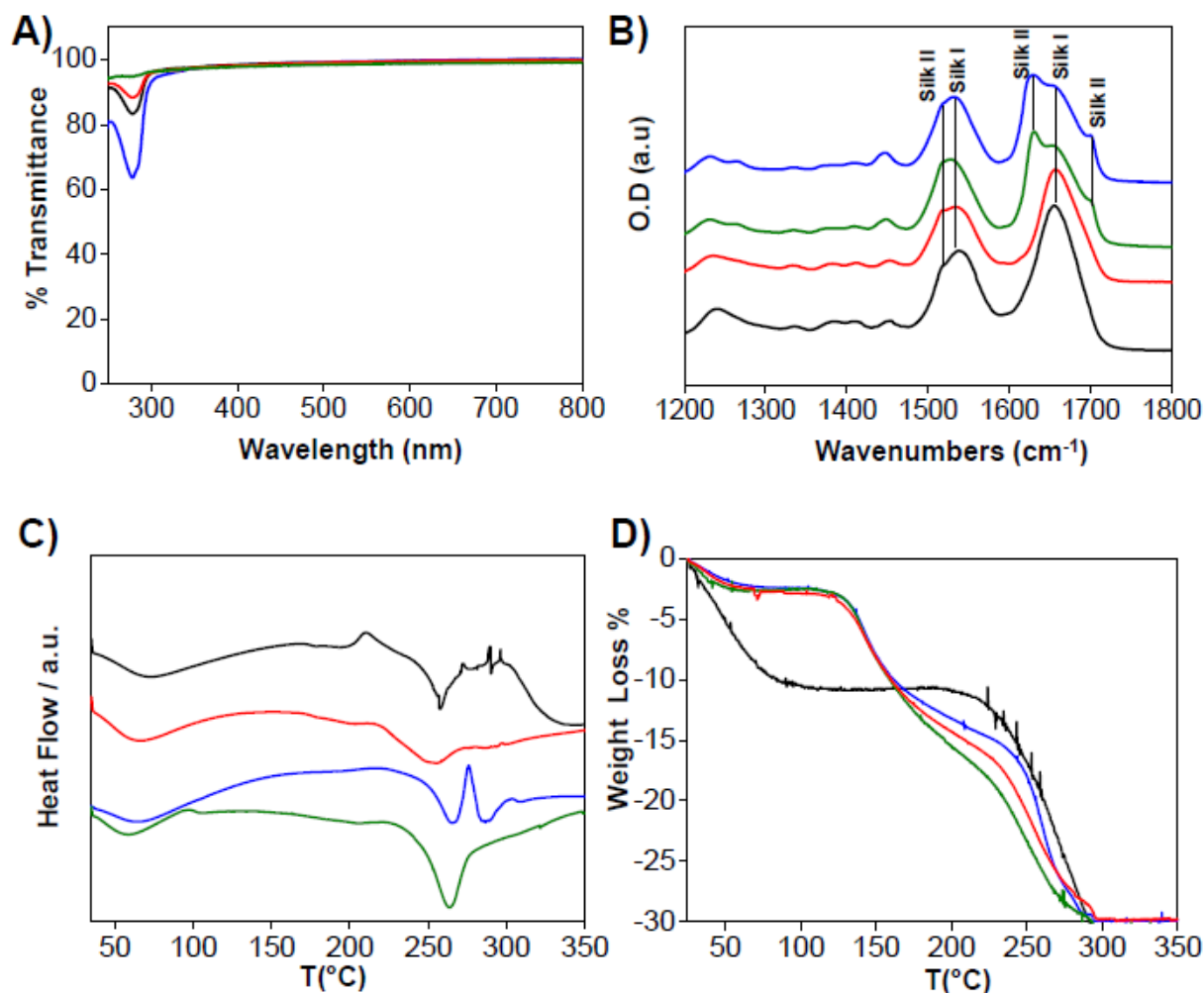
Figure 9. Optical and conformational properties of different RSF films: SF-DC (black line), SF-DO (red line), SF-VD (blue line) and SF-DC/MeOH (green line). Specifically, A) optical transparency of silk films recorded in UV-VIS range (300-800 nm); B) FT-IR vibration absorption spectra collected in amide regions (1200-1800 cm^{-1}), thermal profiles obtained by DSC (C) and TGA (D) analysis.

Silk film biodegradation and dissolution profiles. Several studies[109] have demonstrated that the degradation time of various silk-based biomaterials forms can be controlled by the content of silk II structures. For this reason we tested the resistance towards enzymatic degradation (protease XIV solution) and the rate of dissolution in aqueous DMEM medium of fibroin assembled in different films. Biodegradation experiments were performed incubating RSF films at 37°C with protease XIV solution for 15 days. The rate of degradation was calculated through the loss of weight of fibroin in the films. The results, reported in figure 10A, confirmed a correlation between the content of silk I and silk II structures and the rate of degradation. Indeed, SF-DC and SF-DO films (figure 10A, black and red line, respectively) characterized by the predominance of silk I water-soluble structures lost both ~90% of initial weight after 24 h of incubation. On the other hand, the SF-VD

and SF-DC/MeOH films (figure 10A, blue and green line, respectively), characterized by silk II water-insoluble conformation, showed a lower rate of degradation compared to SF-DC and SF-DO samples. In particular, SF-DC/MeOH film displayed a weight loss of ~70%, ~85% and ~90% after 24 h, 48 h and one week respectively, whereas the SF-VD film showed the lowest rate of degradation losing ~20% after 48 h, ~30% after one week and ~70% after 15 days.

Dissolution profiles, according to biodegradation data, highlighted that the fibroin conformations affected solubility of protein assembled in various films. As shown in figure 10B, SF-DC (black line) and SF-VD (blue line) films revealed the highest and the lowest rate of dissolution in DMEM medium, respectively. Indeed, after 6 h of incubation in DMEM the dissolved percentage of fibroin films was ~95% for SF-DC and < 10% for SF-VD; moreover, for the latter the maximum weight loss was ~20% after 15 days. Regarding the SF-DO and SF-DC/MeOH films (figure 10B, red and green line, respectively), they showed intermediate dissolution profiles in DMEM medium; SF-DO film lost ~70% of weight after 6 h, then a plateau is observed, while SF-DC/MeOH film displayed a lower dissolution rate losing <50% of weight after 6 h and ~55% after 15 days of incubation. It is noteworthy that by increasing the silk II structures, the dissolved silk fibroin amount decreased. The different behaviour in DMEM and in presence of protease of the SF-VD and SF-DC/MeOH films, despite the similar infrared spectra, could be due to the different morphology properties of silk after the different film fabrication.

Notably, by subtracting the weight loss values correlated to dissolution profiles (figure 10B) to those of biodegradation assay (figure 10A) we achieved just enzymatic effect on the silk films degradation process (figure 10C). The results displayed (figure 10C) an increase of protease action corresponding to decrease of dissolution rate of silk film. Indeed, enzymatic degradation effect was lowest (almost zero) and greatest for water-soluble SF-DC (black line) and water-insoluble SF-VD (blue line) films. An intermediate protease effect for SF-DO and SF-DC/MeOH films (red and green line, respectively) was obtained, however it was correlated to major content of silk II structures.
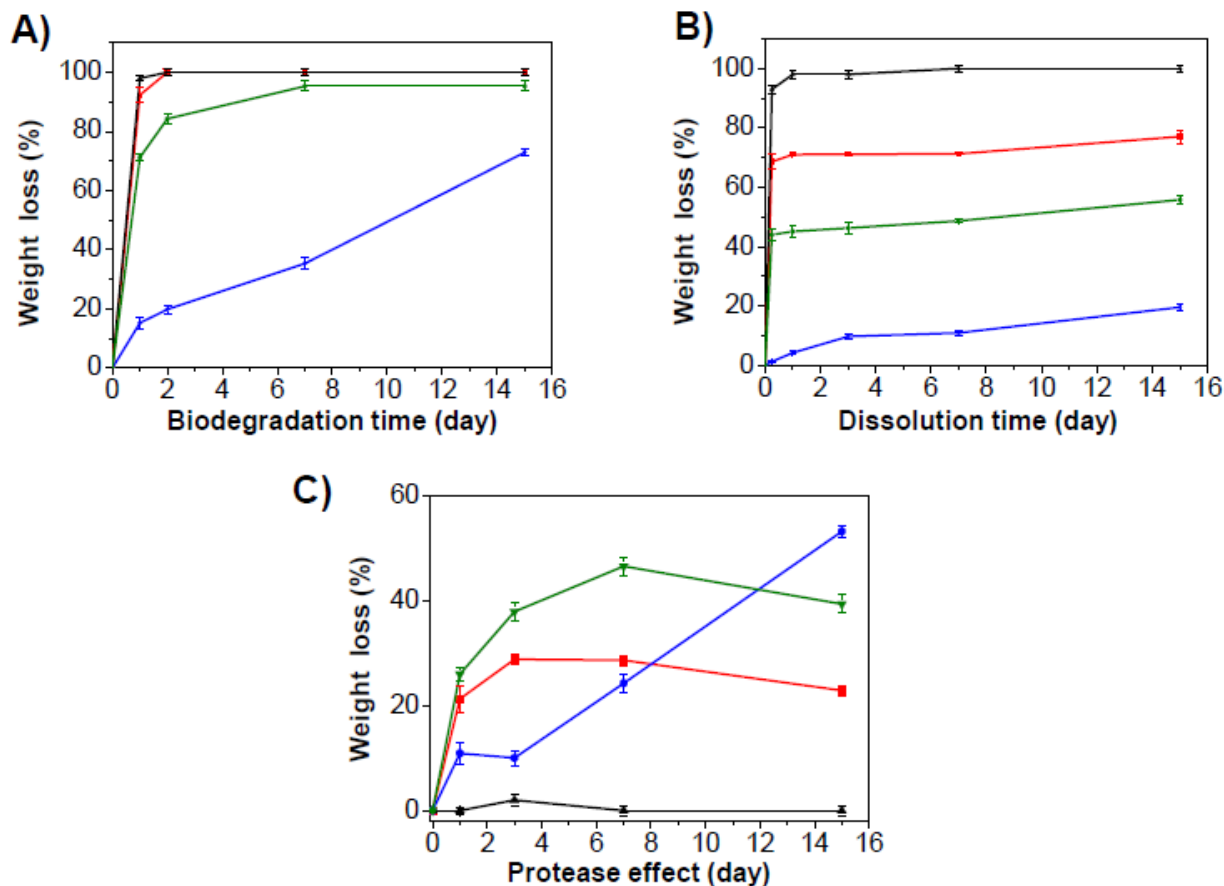
Figure 10. Biodegradation and dissolution profiles of RSF films: SF-DC (black line), SF-DO (red line), SF-VD (blue line) and SF-DC/MeOH (green line). Specifically, A) biodegradation rate of silk films incubated in protease XIV solution at 37°C; B) dissolution time of silk films maintained in aqueous DMEM medium at 37°C; C) enzymatic effect profile on different silk films.

Silk film surface properties and morphological characterization. Attachment and proliferation of cells and tissue biomaterials are dependent upon the surface properties such as topography, nano-roughness and the hydrophobicity/hydrophilicity ratio. Atomic force microscopy (AFM) is a powerful tool to obtain with nanometer spatial resolution direct information about the morphology of a film. AFM images of the various RSF films (figure 11) were collected in order to detect the morphological differences induced by the different approaches used for films fabrication. The sample SF-DC with a secondary structure of the random coil type showed the smoother surface with an average roughness of about 2 nm (figure 11A). The morphology of this film recalls that observed for RSF films obtained using the same drop-casting and slow-drying method.[110] Differently, the SF-VD film (figure 11C), showing the increased content in β-sheet and the higher hydrophobicity, is the one with the greater roughness (~51 nm), however, the grainy morphology is similar to that of the SF-DC sample. The films treated with methanol (SF-DC/MeOH) and dried in

the oven (SF-DO) showed intermediate roughness values (~29 nm and ~15 nm, respectively) with a completely different morphology (figure 11B and 11D, respectively). In particular, the SF-DO film is characterized by little holes and small aggregates of protein; in this case, the drying process at 50°C does not affect the conformational structure of the protein that is similar to that of SF-DC sample (silk I conformation) but influences the morphology of the SF film surface. At the end, the SF-DC/MeOH sample shows a morphology totally different to that of the SF-VD film with the same secondary structure (β-sheet type); indeed, the surface presents the highest degree of molecular aggregation suggesting that methanol treatment could promote a more packed protein structure (increase of crystallinity index).[110] The different morphology and features of the four analyzed films are probably due to the different molecular motion of the protein induced by the different conditions of water evaporation used for films preparation.
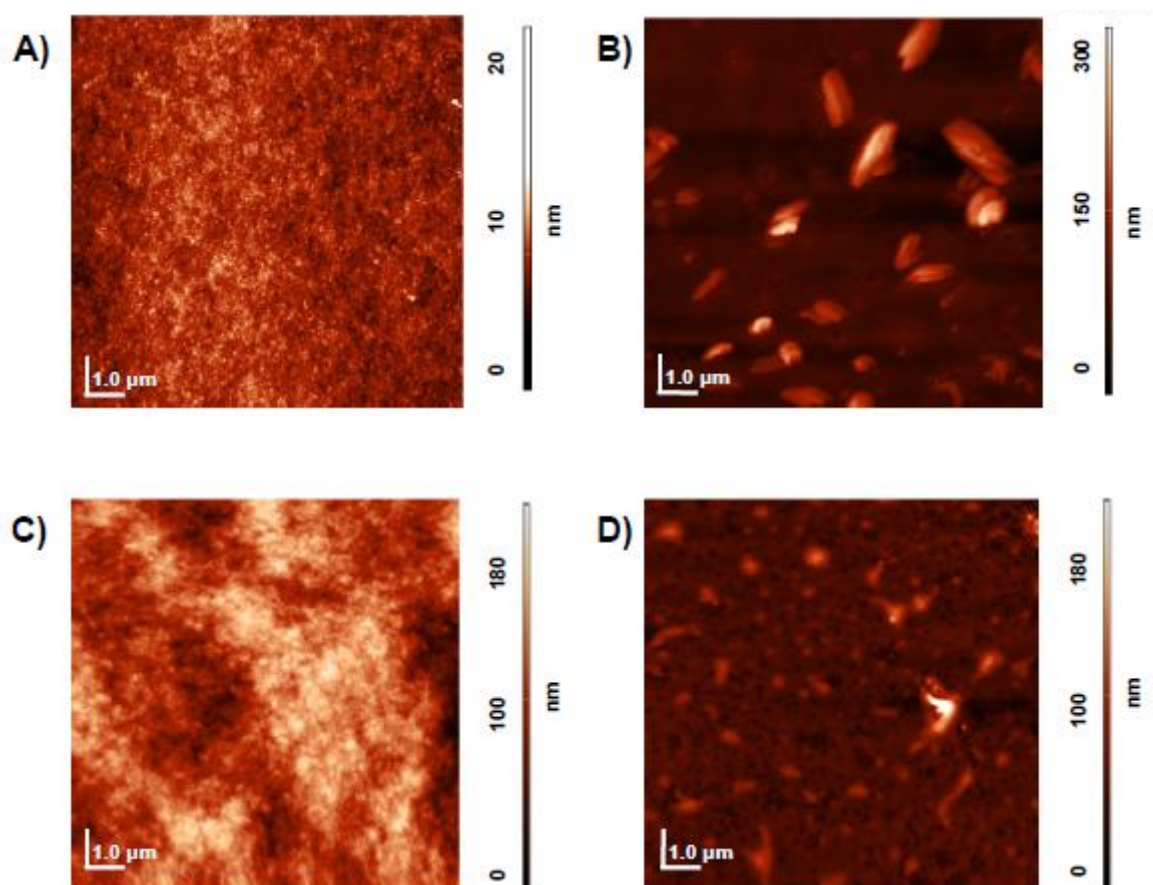
Figure 11. AFM topographical images of RSF films obtained using different methods: A) SF-DC untreated (RMS~3.13 nm) and B) treated in MeOH (RMS~23.35 nm) films, C) SF-VD (RMS~12.37 nm) and D) SF-DO (RMS~11.4nm) films.

Recent studies demonstrated that surface modifications of SF films can be used to enable controlled adsorption of proteins and regulated cell-proliferation.[111] In this view, DMEM medium contact

measurements were performed in order to investigate the surface properties of different RSF films. As reported in table 3, the SF-DC film (figure 12A) showed a low value of contact angle (~ 39.1°) attributed to a major hydrophilicity of the surface. The increase of contact angle value for the SF-DO, SF-DC/MeOH and SF-VD films (~ 45.9°, ~ 53.9° and ~65.8°, respectively) indicated instead an increase of hydrophobicity of the different SF substrates (figure 12B-D), especially with regard to the SF-VD sample (figure 12D). The hydrophilicity/hydrophobicity of a surface is related to its wettability; therefore the hydrophobicity increased, while the wetting of samples decreased. This is correlated to the different dissolution profiles observed for the SF films (see table 3 and figure 10B). In fact, the most hydrophobic SF-VD film is the one that dissolves and degrades more slowly differently to the more hydrophilic SF-DC film.

	SF-DC	SF-DO	SF-DC/MeOH	SF-DV
CA (degree)	39.1 ± 0.45	45.9 ± 0.30	53.9 ± 0.25	65.8 ± 0.80

Table 3. Contact angle (CA) values for a DMEM medium droplet (1 mL) spreading on surface of different RSF films.
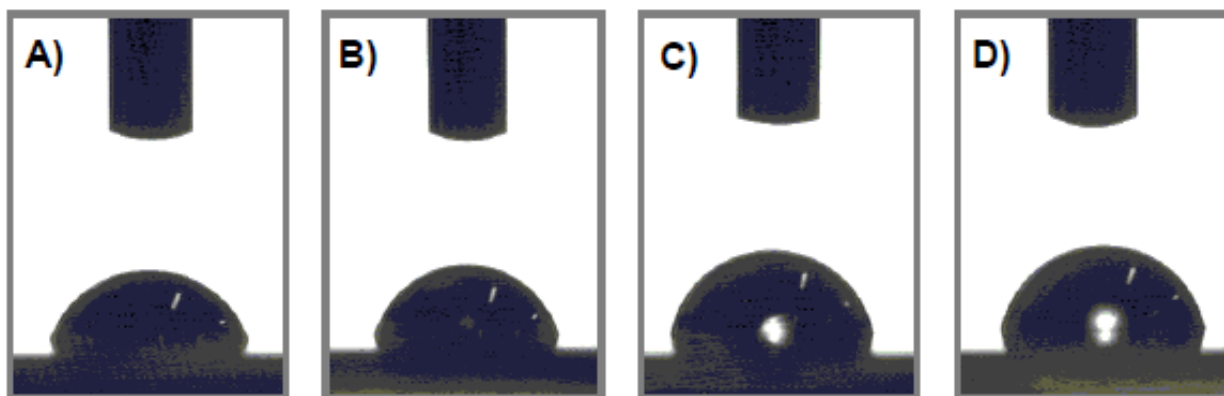
Figure 12. Contact angle measurements of RSF films. Shapes of a DMEM medium droplet (1 mL) on the surface of RSF films prepared on glass substrate by different methods: A) DC, B) DO, C) DC/MeOH and D) VD.

Silk film mechanical properties. Flexibility and robustness of silk films were analyzed by stress-stain tests. As reported in table 4, the value of tensile modulus of different RSF films increases as a consequence of an increase in β-sheets content, indicating a mechanical stability due to the major amount of physical cross-links between fibroin chains. These results show that the mechanical properties of silk films can be controlled by different processing approaches.

	E / MPa	Stress at break / Nmm^{-2}	Elongation at break /%
SF-VD	3815±104	67.1±6.0	2.82±0.21
SF-DO	2562±96	68.8±7.2	2.96±0.59
SF-DC/MeOH	3262±170	68.6±2.1	2.16±0.07
SF-DC	2575±23	76.5±0.4	3.39±0.47

Table 4. Mechanical properties of silk film prepared by different processes.

We demonstrated that water-insoluble and stable silk films, with high content of silk II structures, can be fabricated by the Vertical Deposition method avoiding the use of organic solvent. Biodegradability of silk films fabricated by VD process can pave the way to formation of new protein-based biomaterials used in a wide range of biomedical applications, including drug delivery.

4.3 Properties of innovative multifunctional silk fibroin nanocomposite films

Bio-nanocomposites are organic-inorganic hybrid nanostructured materials with synergistic properties arising from the combination of biopolymers and inorganic components. The multifunctionalities of bio-nanocomposites make them very attractive for applications in different fields including packaging, catalysis, optics, electronics, biomedicine, tissue engineering and drug delivery.[112-114] Inorganic fillers such as silica, titania, zirconia, apatite, carbon nanotubes, or metal nanoparticles have been utilized as reinforcing agents in order to improve properties of silk films.[115,116] With the aim to include additional functionalities to silk fibroin and to modulate its mechanical and biofunctional properties, during the second year of my PhD we developed and characterized two innovative silk fibroin nanocomposites: SF-Hydrotalcyte and SF-Single Walled Carbon Nanotubes. Results have been published in references 79 and 87, respectively. A summary of the results that I contributed to reach these goals are reported below.

4.3.1 SF-Hydrotalcyte bionanocomposite

Hydrotalcite-like compounds (HTlc) or layered double hydroxide (LDHs) are an important layered matrix represented by the general formula $[M(II)_{1-x}M(III)_x(OH)_2]^{x+}[A^{n-}_{x/n}]$ mH_2O where M(II) is a divalent cation such as Mg, Ni, Zn, Cu, or Co, M(III) is a trivalent cation such as Al, Cr, Fe, or Ga,

and An$^-$ is an anion of charge n.[117] HTlc are the only example of layered solids with positively charged layers and exchangeable interlayer anions to maintain charge neutrality. The interlayer anions can be exchanged by other inorganic, metallorganic, or organic anions and by biomolecules.[118] HTlc thanks to low toxicity and good biocompatibility are used in biological and pharmaceutical fields for controlled storage and release of active species intercalated in layered materials. Because of their tunable layered charge density and chemical composition HTlc can be used in nanocomposite for drug release.[119]

In this context, a SF-HTlc composite was fabricated by using a completely water-based process (see Materials and Methods, section 3.4 and figure 13A) and its properties were widely investigated; our studies are reported in the literature[79] and the main results are discussed below.

HTlc nanoplatelets having the formula $[Zn_{0.72}Al_{0.28}(OH)_2]^- Br_{0.28}$ 0.69 H_2O were synthesized in the form of colloidal aqueous dispersion according to published methods.[120] TEM and AFM studies revealed that the product of synthesis were nanoparticles whose dimensions are 150−200 nm in width and 20−30 nm in hight.[120] The zeta potential of HTlc colloidal dispersion in water (pH 7.0) was +50 mV.48.
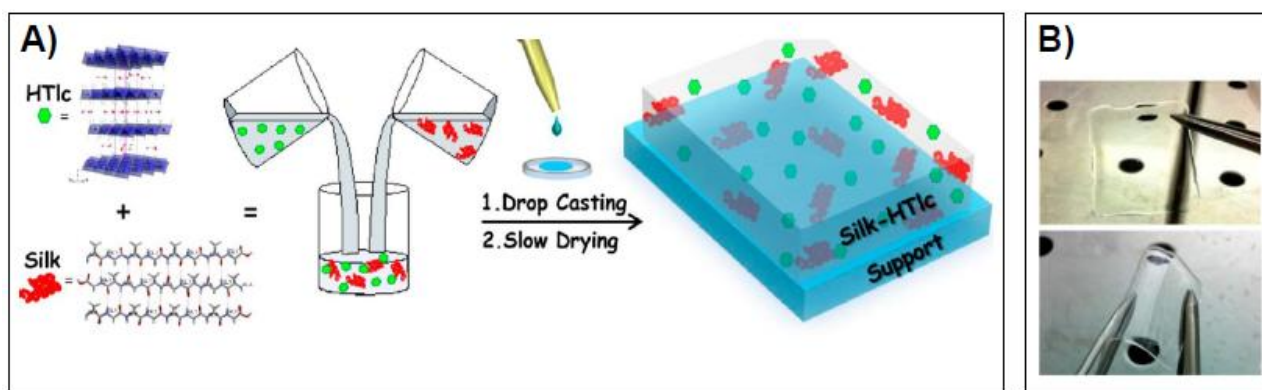
Figure 13. A) Schematic representation of the manufacturing of SF-HTlc hybrid water-solution and films. B) Pictures of a transparent, free-standing and flexible SF-HTlc bionanocomposite film.

Free-standing and flexible hybrid films (figure 13B) were processed from environmentally friendly aqueous solutions. We first prepared bio-nanocomposite by mixing the RSF solution and colloidal nanoparticles aqueous dispersion in different percentages (wt/wt%). The SF-HTlc film was prepared from the hybrid dispersion by DC method (details in Material and Methods section and in references 79). The resulting film was optically transparent and displayed enhanced mechanical properties with respect to bare SF.[79]

FT-IR experiments were carried out in order to investigate the structural properties of silk protein after incorporation of HTlc nanoparticles. Spectral features of the HTlc and silk samples (figure 14A and 14B), observed in the 400−3800 cm^{-1} frequency range, recall those reported for other conventional hydrotalcite[121] and regenerated SF film prepared by DC method. Figure 14A shows that amide I (1655 cm^{-1}), amide II (1535 cm^{-1}) and amide III (1240 cm^{-1}) bands, corresponding to the SF-HTlc nanocomposites, match well with those observed in pure protein films, suggesting an unaltered protein structure after incorporation of HTlc nanoparticles. Furthermore, the band positions are mainly indicative of the water-soluble silk I conformation that is typical of SF films obtained by the same DC process. FT-IR spectra recorded for SF-HTlc hybrid films show together with the bands assigned to the silk protein other signals in the 3250−3500 cm^{-1} and below 1000 cm^{-1} regions, characteristic of these layered materials (figure 14B).

A high-frequency shift (612 cm^{-1}) of the band at 601 cm^{-1} is detected in SF-HTlc nanocomposites which is almost independent from the hydrotalcite content. The observed blue shift (up to 10 cm^{-1}) could be ascribed to the existence of interactions between the protein and hydroxyl groups of HTlc layers. It is possible that OH groups of HTlc form hydrogen bonding with C=O and NH groups of silk fibroin aminoacids.
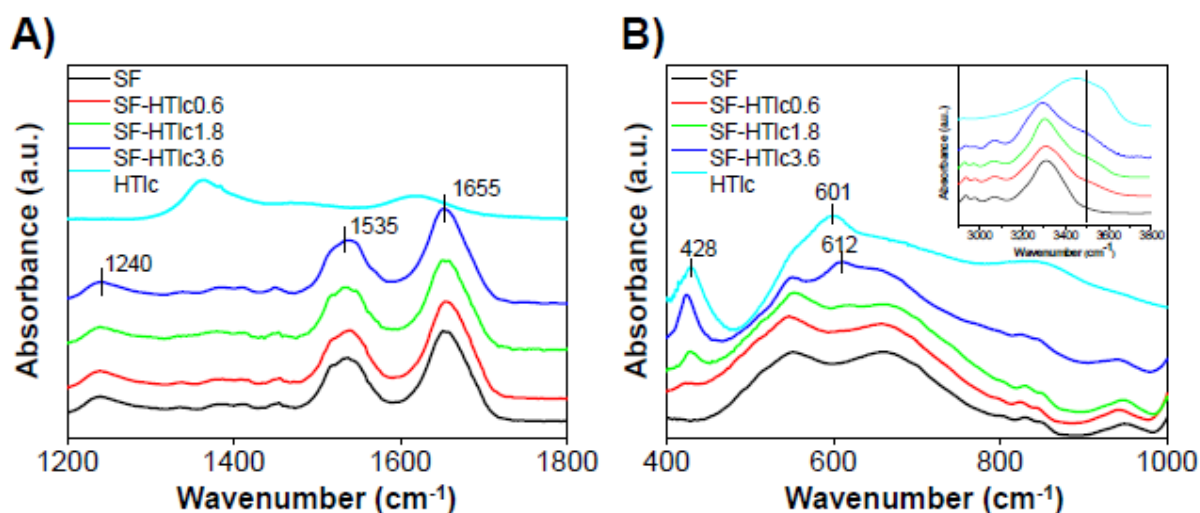
Figure 14. FT-IR spectra of pure SF film (black line), HTlc nanoparticles in powder form (cyan line), and SF-HTlc hybrid films recorded in the 1200−1800 cm^{-1} region (A) and 400−1000 cm^{-1} region (B). The inset of (B) shows the bands relative to the 3000−3800 cm^{-1} region.

The dispersion degree of the HTlc nanoparticles into the silk matrix and the morphology of the nanocomposite films have been investigated by optical microscopy, AFM and SEM-EDS analyses.[79]

The elemental mappings of Zn and Al in silk hybrid films containing two different percentages of HTlc (SF-HTlc0.6 and SF-HTlc3.6 samples) were obtained by a SEM-EDS technique and are presented in figure 15. The density of each element is indicated by the relative brightness and colour intensity and corresponds with its composition within the samples (figure 15A−C middle and right panels). Overall, these two elements exhibit an homogeneous distribution of density both on the surface (figure 15A-B) and in the entire thickness (figure 15C) of the hybrid composites under examination (SF-HTlc3.6). It can be observed that increasing the weight percentage of HTlc in the composites, the relative densities of Al^{3+} and Zn^{2+} change accordingly. Summarizing optical microscopy, AFM,[79] and SEM images indicated a homogeneous integration of the HTlc nanoplatelets into the silk matrix.
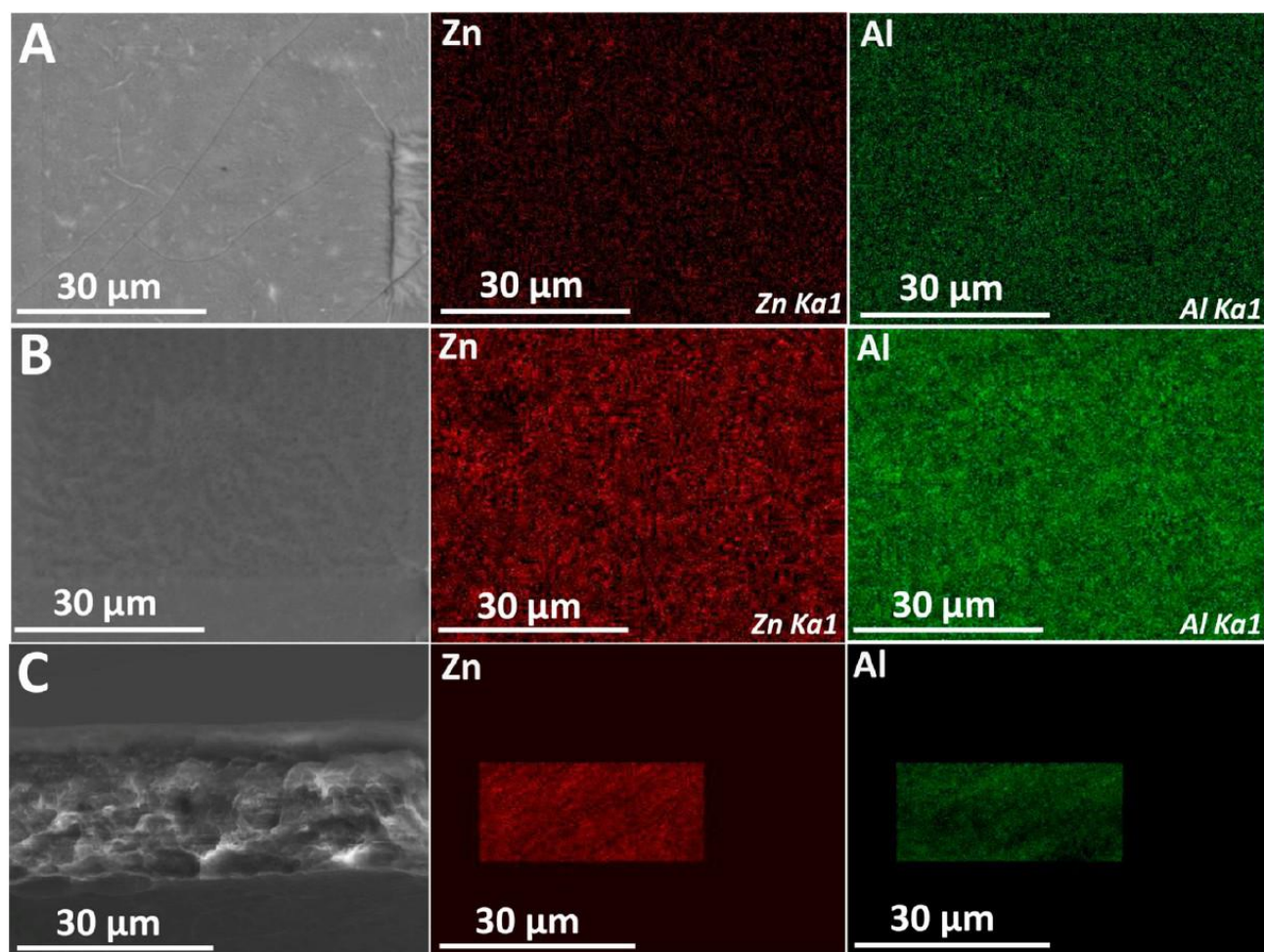
Figure 15. SEM images and the corresponding EDS images of Zn and Al elements in samples SF HTlc0.6 (A), SF-HTlc3.6 (B), and in the section of SF-HTlc3.6 (C). It is interesting to note that the thickness of the sample SF-HTlc3.6 measured by SEM (~18 μm) is similar to that measured by profilometer.[79]

Biodegradation of fibroin in SF-HTlc composite films. Figure 16A shows the *in vitro* degradation of pure SF and SF-HTlc hybrid films incubated at 37°C with protease XIV solution (1mg/mL in PBS). The rate of degradation was calculated through the loss of weight of fibroin in the films. The SF film shows a rapid weight loss of ~90% after 1 day of exposure to protease that is almost complete after 2 days of incubation; the same weight loss is observed for SF-HTlc0.6 sample indicating that a small amount of HTlc nanoparticles does not affect the degradation process of SF. Differently, the SF-HTlc1.2 and SFHTlc1.8 nanocomposites show a particular trend: after 1 day of incubation a weight loss of only 40−60% is observed and the 80% of loss is reached after 4 days. This finding suggests that HTlc nanoparticles in a particular range of concentration have the ability to protect SF from enzyme attack. On the other hand, the behavior of SF-HTlc3.6 sample recalls that of the pure SF film.

As previously (section 4.2) discussed and illustrated, silk fibroin is susceptible to biological degradation by proteolytic enzymes; the rate and extent of degradation may be highly variable depending on the structural and morphological features of the polymer (fiber, film, sponge) and the processing conditions. The β-sheet structure (silk II conformation) is considered to be a critical factor that stabilized SF in aqueous environments. Because the secondary structures of SF do not change in SF-HTlc nanocomposite (see figure 14A), the results here reported suggest that the increased protease resistance of SF is due to the excellent dispersion of HTlc nanocrystals in the silk matrix. The dispersed platelets could potentially cover the access of the protease to its binding sites, acting as a physical barrier to protease attack.

Dissolution of HTlc in SF-HTlc composite films. It is known that hydrotalcite-type materials are basic compounds that rapidly dissolve in acidic media.[117] Figure 16B shows the dissolution profiles in phosphate buffer at pH 3.0 of HTlc, pure SF and SF-HTlc1.8 nanocomposite films, chosen because it was in the range of SF-HTlc nanocomposites with enhanced mechanical properties.[79] HTlc film shows 100% of weight loss almost instantaneously, while SF and SF-HTlc1.8 hybrid films exhibit a much slower and comparable dissolution process. After 3 h of incubation, only a 7−10% of weight is lost reaching the 20−30% in 2 days, indicating a good stability of the SF and SF-HTlc1.8 films in acidic medium. These results demonstrated the protective effect of SF by detrimental interaction of HTlc with harsh acidic pH environment.

Collectively, our results demonstrated that a mutual benefit effect on the stability of both organic and inorganic components was observed in the nanocomposites. SF-HTlc displayed limited

dissolution of hydrotalcite in acidic medium, enhanced mechanical properties and higher protease resistance of silk protein. These data are very attractive for applications in biomedicine and in innovative drug delivery formulations.
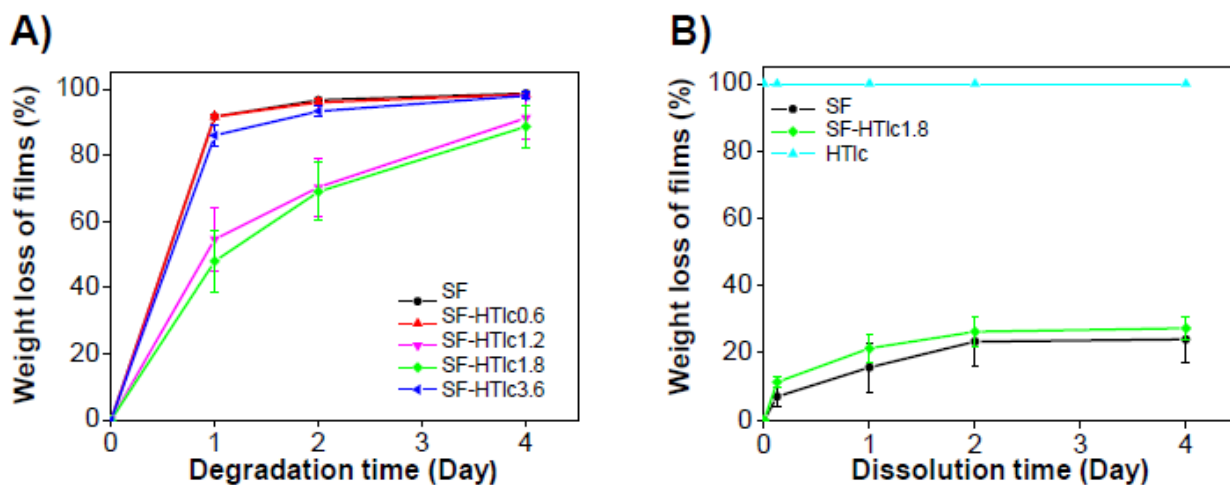
Figure 16. A) Enzymatic degradation profiles of pure SF film (black line) and SF-HTlc nanocomposites. Regenerated SF and SF-HTlc hybrid films were cultivated in protease XIV solution. B) Dissolution profiles of pure SF film (black line), SF-HTlc1.8 hybrid film (green line) and pristine HTlc film (cyan line) in phosphate buffer at pH 3.0.

4.3.2 Nanostructured silk fibroin–single walled carbon nanotubes composite

Single Walled Carbon Nanotubes (SWCNTs) represent the most appealing class among conductive nano-materials for biomedical applications.[122] They have unique physical and chemical properties, which enable the development of high capacitance, low-resistance nanostructured electrodes, that are potentially useful for cell interfacing and modulating cell activity i.e. for neural prosthetics.[123]

In this context we generated a conductive[87] nanostructured (n) SF–SWCNTs film by using the same fabrication method applied in order to produce three-dimensional (3D) ordered structures of interconnected submicrometric pores of SWCNTs.

The structural, electrical, conformational, mechanical properties and the biocompatibility with primary dorsal root ganglion neuronal cells (DRG) of the SF-SWCNTs nanocomposite film were investigated. Results of our studies have been published in reference 87 and summarized below.

We assembled SWCNTs in periodic structures by using polystyrene beads (PB), which acted as both carriers and a sacrificial template. These structures were then infiltrated by RSF water-solution. This preparation method is extremely versatile and allows us to tune the periodicity of the SF–SWCNT porous structure by controlling the templating bead diameter.[93] We used the microfluidic VD method to deposit the template made of SWCNTs on 415±10 nm sized PB. A

defined volume of RSF water-solution was infiltrated into the template by DC approach. Afterwards the PB templates were dissolved by a gentle solvent treatment.
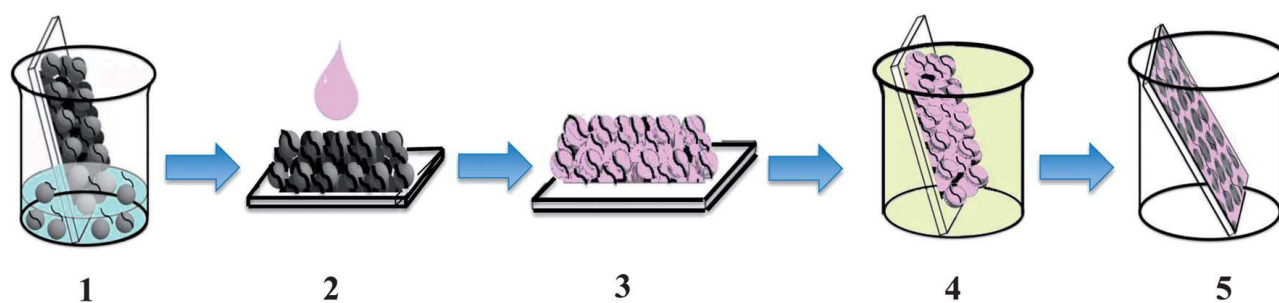
Figure 17. Fabrication scheme of porous hybrid films of nSF–SWCNT: (1) VD of the PB and SWCNTs; (2 and 3) SF infiltration into the ordered PB–SWCNT structure by DC; (4) template removal by solvent treatment; (5) final hybrid nSF–SWCNT composite after rinsing in ethanol.

Morphological characteristics. SEM imaging revealed a 3D geometrically controlled structure of nSF–SWCNT composites (figure 18A). The inverse structures resulted in nanostructured hybrid films of SWCNTs completely embedded in SF with an average thickness of around 1 mm. The films had regular pores of 315 ±40 nm in diameter, assembled in a close packing array (figure 18A). The pores were completely 3-dimensionally interconnected by windows of 90 nm.

Fibroin conformation in nSF-SWCNTs composite film. The SF conformation was investigated by IR spectroscopy, within the range 1700–1200 cm^{-1}, for both bare nanostructured SF (nSF) and the nSF–SWCNT composite (figure 18B). In the IR spectrum of nSF–SWCNT none of the observed peaks can be attributed to the nanotubes because the IR absorption cross section is much smaller for the SWCNTs than for nSF. SF-SWCNTs composite film (figure 18B, red line) shows the typical signals of the silk I structure and match well with the spectrum of a non-nanostructured SF film. Specifically, the amide I band appeared as a strong peak at 1655 cm^{-1}, corresponding to the silk I structure; in the amide II region, peaks are observed at 1535 cm^{-1} (silk I) and 1517 cm^{-1} (silk II); in the amide III region a peak at 1240 cm^{-1}, generally assigned to random coil-structures, is observed.

These data indicate that the conformational structure of the protein is not modified in the nSF–SWCNT composite with respect to nSF and the dominance of the silk I structure (random coils and α-helices) over silk II (β-sheets) is maintained after all of the preparation processes that nSF goes through.

Structural properties of SWCNT in nSF-SWCNTs composite film. The Raman scattering spectra collected for the nSF–SWCNT films (figure 18C-D) are dominated by the SWCNT scattering, exciting at both 488 nm in the blue and 632.8 nm in the red. No significant differences were observed among the spectra collected for the nSWCNT and nSF–SWCNT substrates. Minimal differences were detected in the relative intensities of the RBM, D, G, G0 modes; these variations are related to the distribution of different nanotubes in both samples and not to the presence of SF. The Raman scattering for nSF at both of these excitation wavelengths is very weak and all of the peaks are in the same regions as the peaks attributed to SWCNTs (the spectra of SF in figure 18C-D were carried out on a very thick film compared to nSF–SWCNTs and further reduced in intensity compared to the spectra of the other compounds). The presence of a broad band around 2900 cm^{-1} in the spectra of nSWCNTs (probably due to the C–H bonds formed on the nanotubes during the cleaning and solubilization processes), does neither allow to clearly identify the Raman spectra of nSF–SWCNTs nor the most intense Raman peaks for SF (C–H stretching at 2940 cm^{-1}).
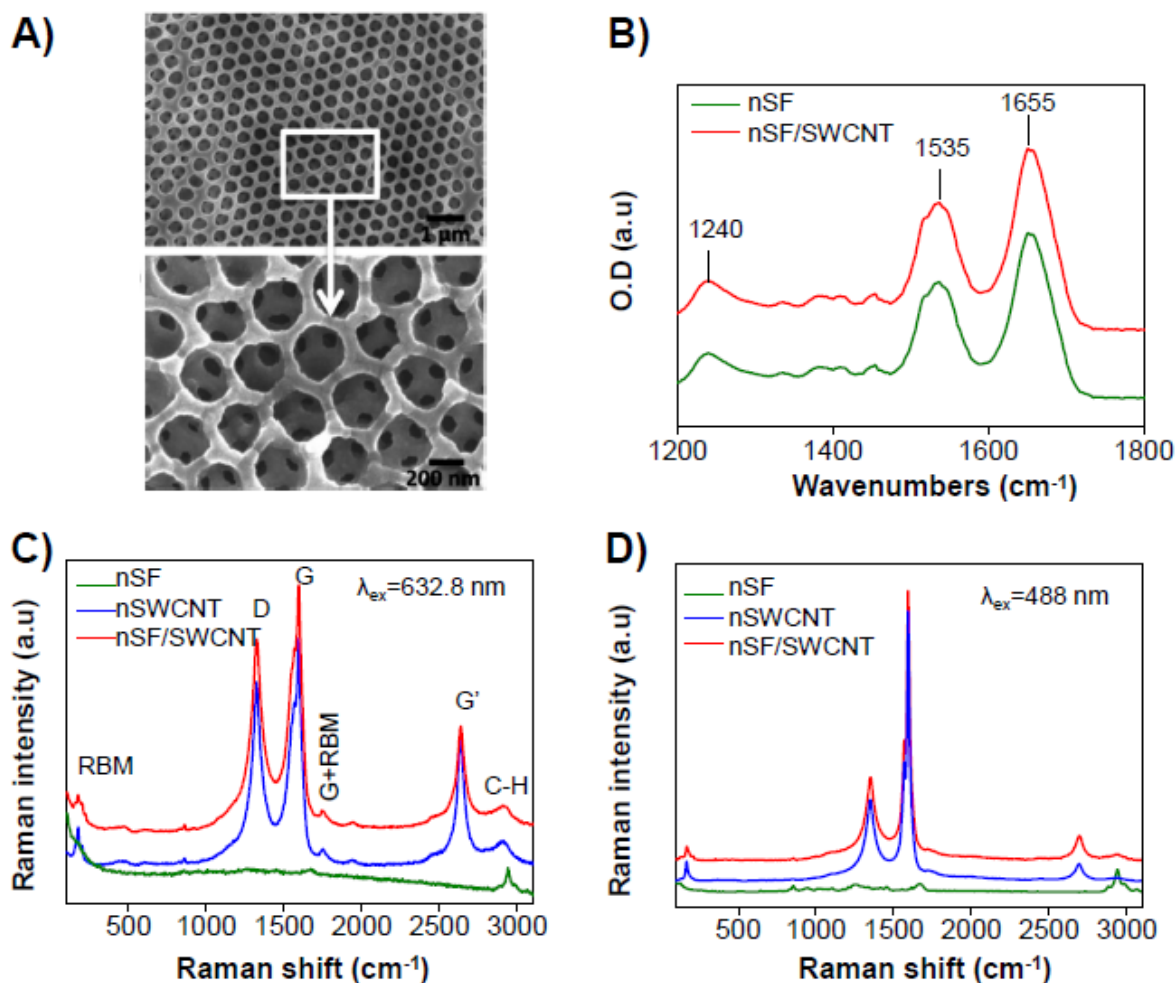
Figure 18. A) SEM micrographs of a nSF–SWCNT porous film at different magnifications. B) Infrared spectra of nSF–SWCNT and nSF films deposited on a glass substrate. C-D) Raman spectra of nSF–SWCNT, nSWCNT and SF exciting at 632.8 nm (C) and at 488 nm (D).

Biocompatibility with primary DRG neurons. Biocompatibility is an essential feature to be carefully evaluated and considered as an advanced function of a novel engineered bionanocomposite. A biocompatible nanocomposite could be potentially used to promote and guide neurite outgrowth, as well as to stimulate functional recovery of injured neurons, representing a crucial tool in neuronal regenerative medicine and nerve repair.[124]

We evaluated the biocompatibility of the nSF–SWCNT substrate by culturing primary rat DRG neurons on nSF–SWCNTs and on nSF for several days. We chose to use cultures of dissociated rat DRG neurons as it is a validated *in vitro* model to determine the regenerative outgrowth capabilities of individual neurons of the PNS. The DRG cell culture behaviour on bare non-nanostructured SF has been fully characterized morphologically, immunologically and functionally in our previous work, thus it is a good benchmark control.[14]

Neural cell viability and neurite outgrowth were analyzed by optical microscopy with Fluorescein Diacetate (FDA) assay and by fluorescent microscopy (figure 19A). A histogram plot of the mean FDA-positive cell n°/area reveals that the viability of the conductive nSF–SWCNT substrate is comparable to that of nSF (figure 19B).

Additionally, the mean neurite length of the DRG neurons grown on the nSF–SWCNT nanocomposite, after 3 DIV and 10 DIV is also comparable to that of nSF (figure 19B). These results suggest that the cells grown on the nanocomposite mostly directly interact with the substrate at the nSF/cell interface, rather than with the SWCNTs, potentially reducing the biocompatibility issues related to SWCNTs.[125]

Collectively, these data show that the nSF–SWCNT nanocomposite is a permissive neuron interface that enables DRG neuron adhesion and differentiation *in vitro*.
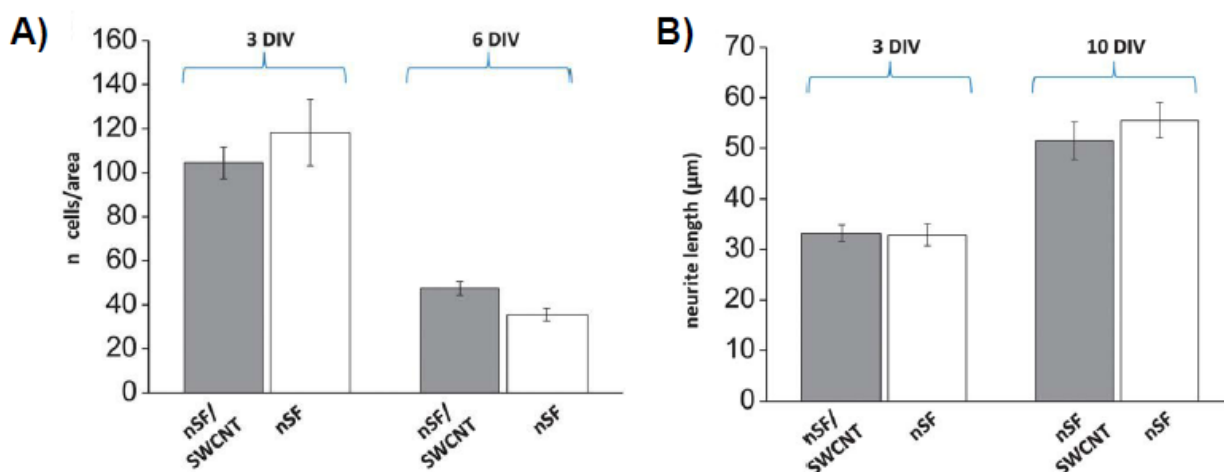
Figure 19. Biocompatibility of the nSF–SWCNT nanocomposite. A) Histogram plot of the number of FDA positive cells/area counted in cell culture preparations grown on nSF–SWCNTs (gray bars), and nSF (white bars), after 3 and 6 days *in vitro* (DIV). B) Histogram plot showing the neurite length measured of neurons grown on nSF–SWCNTs (gray bars) and nSF (white bars), after 3 and 10 days *in vitro* (DIV).

4.4 Innovative methods of functionalization of silk fibroin solution and films

In order to widen the potential of *B. mori* RSF and its applicability,[70,75,126] different doping methods of silk solution, water chemical tailoring approaches relying on site specific covalent modification[72,73] and supramolecular non-covalent interaction have been proposed.[79,87] However, some chemical and physical post-processing treatments of SF could damage/denature the protein, modifying completely its primary properties and in turn the properties of the films. Independent from the approach, mild and water compatible procedures as well as water soluble reagents are

required in order to effectively perform protein doping and to prevent SF denaturation or detrimental structural changes.

In this context, during the third year of my PhD, we developed two innovative doping methods of functionalization of the silk fibroin solution and films: **1)** Biodoping and **2)** Silylation.

Regarding *biodoping*, the results of our studies are published in reference 80 and are illustrated below.

4.4.1 Biodoping of silk fibroin fibres, solutions and films.

Recently, a series of fluorescent dyes have successfully been incorporated in silk fibres by the addition of colorant compounds to the silkworm diet. In particular, Tansil et al. [94,95] mixed Rhodamine B (RhB) into mulberry powder at different concentrations to make modified feed for the silkworms at the third day of the fifth instar. They showed that successful formation of pink and luminescent (under UV irradiation) cocoons and silk threads could be obtained with different intensity in colour and luminescence depending on the concentration of RhB in the diet. The body of the silkworms and the fibres assumed a pink colour and the biodistribution study of xenobiotic in *B. mori* revealed an uptake of RhB in the native fibroin solution of the prothoracic gland. [94,95]

However, possible effects of extraction and preparation on chemo-physical properties of the RSF solution and films from the modified diet cocoon were not investigated. Considering that several passages of the extraction and purification processes could compromise efficient inclusion of the doping molecules in the final silk-based substrates, we characterized the chemo-physical properties of RSF solutions and films extracted from the cocoon obtained by the RhB-modified diet (RhB-md) method.[80] The first step of our study was to feed a polyhybrid strain of *B. mori* (figure 20A) with RhB according to the protocol of Tansil et al. [94,95]

In particular, RhB was mixed into the artificial powder diet at a concentration of 0.05 wt% to make a modified feed that was then fed to silkworms starting from the third day of the fifth instar (figure 20B). To monitor the correlation of RhB inclusion in the cocoon with the time of exposure to the diet, 3 groups of white strains, each composed of twenty last instar larvae, were placed in a separated box and fed with the modified diet starting from the third, fourth and fifth day of the fifth instar, respectively, until the silkworms started spinning the cocoon. In this way, we obtained different add-eat time cocoon of 24, 48 and 72 hours (figure 20D-F).

The silkworms fifth larval stage takes about six days; thus, to obtain a different exposure time to the dye, the doped diet was administered on different days from the last molting, from the third, fourth and fifth day until the silkworm starts to spin the cocoon. In the same manner, three groups of the

same strains fifth instar larvae were separated and fed with the same diet, except for the addition of RhB powder, and white cocoons were used as a control (figure 20C).

According to the observation of Tansil et al., [94,95] the body of the worm fed with the RhB-modified diet, became coloured after 2–3 h following RhB diet consumption. Aside from the colour, no difference (i.e. morphology and weight) was observed between the coloured and white cocoons that were produced by the silkworms consuming normal non modified feed.
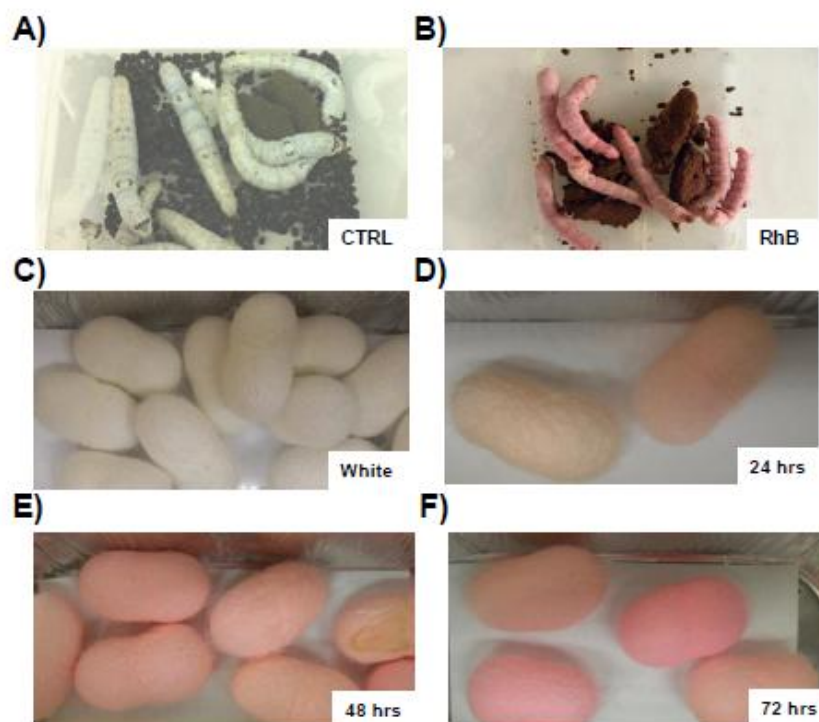
Figure 20. A-B) Larvae of *B. mori* domesticated on standard diet (A) and doped diet with RhB (B). C) Cocoons from silkworms of *B. mori* fed with no doped diet. D-F) Natural coloured cocoons from silkworms fed with diet containing dye. Different rose shades due to time of exposure of larvae to diet (24, 48, 72 hours)

Coloured and white cocoons are degummed as previously described (see section 4.1). After the degumming procedure, the resulting RhB-md-SF fibres (figure 21A, right panels) were coloured with respect to those obtained from white cocoon (figure 21A, left panel) and displayed different shades of violet depending on the exposure time of the worms to the RhB-modified diet. The same gradient difference in colour from the white, 24h, 48h and 72h RhB-modified diet cocoon was evident when RSF fibres were melted in LiBr (figure 21B) and after the purification procedure (dialyses and centrifugation) (figure 21C), by indicating that both degummed silk fibre and regenerated silk solution retain the doping agent.
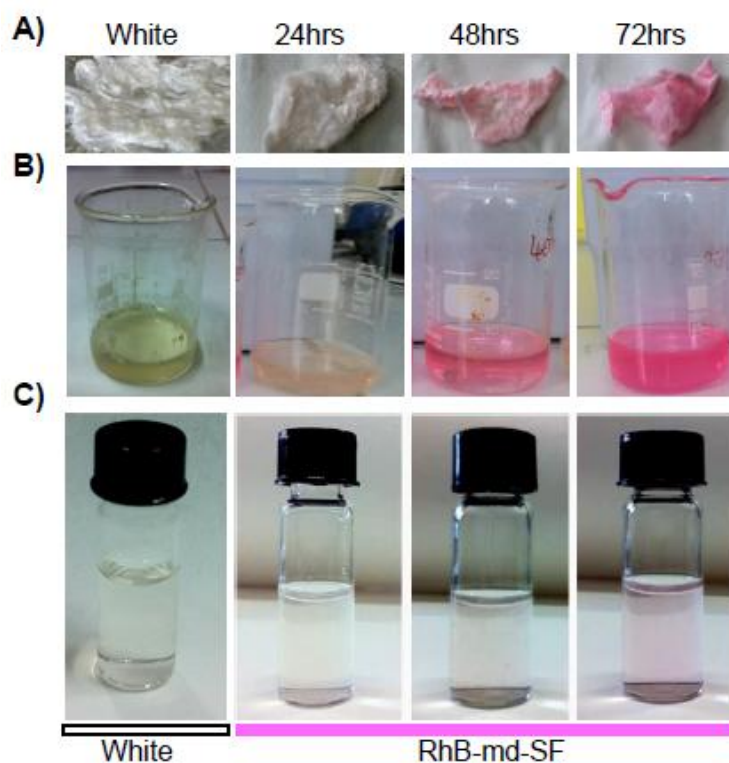
Figure 21. A) Degummed silk fibres obtained from white and RhB-modified diet cocoons (reported in figure 20C-F). B) SF solubilized in LiBr solution. C) RSF solutions extracted from white and RhB-modified diet fibres.

Chemo-physical properties of biodoped silk fibroin solution and films. The main aim of these studies was to analyse the chemo-physical properties of RSF solutions and films obtained from 24h, 48h and 72h RhB-modified diet cocoon to explore the suitability of the *modified diet* method for the biomanufacturing of silk-based optically active substrates in opto-electronic devices. First, we investigated the UV-VIS optical properties of the RSF solutions obtained from white (figure 20C) and coloured cocoons feed for 24h, 48h and 72 h RhB-modified diet (figure 20D-F).

Figure 22 shows the UV-VIS absorption spectra of white and RhB-md-SF solutions obtained in the 300–800 nm range. All RhB-md-SF water-solutions displayed two main features in UV-VIS absorption spectra: a shoulder at 325 nm (figure 22A), and a more pronounced peak at 546 nm (figure 22A-B), whereas for the white SF solution, only the absorbance at 325 nm appeared. The absorbance at 325 nm could be attributed to a small percentage of β-sheets structures.[51] The absorbance at 546 nm, associated with the chromophore group of RhB,[127] increased gradually from RhB-md-SF 24h to RhB-md-SF 72h. In particular, the intensity values were almost proportional to the feeding time (24 > 48 > 72 hours) (figure 22C). When a white SF solution was doped with RhB (RhB-d-SF), it displayed the maximum absorbance at 557 (figure 22D). Therefore, the results of the

UV-VIS absorption of the RhB-md-SF solutions displayed the features of RhB. However, we observed that RhB has a slightly different optical behaviour depending upon the solvent.
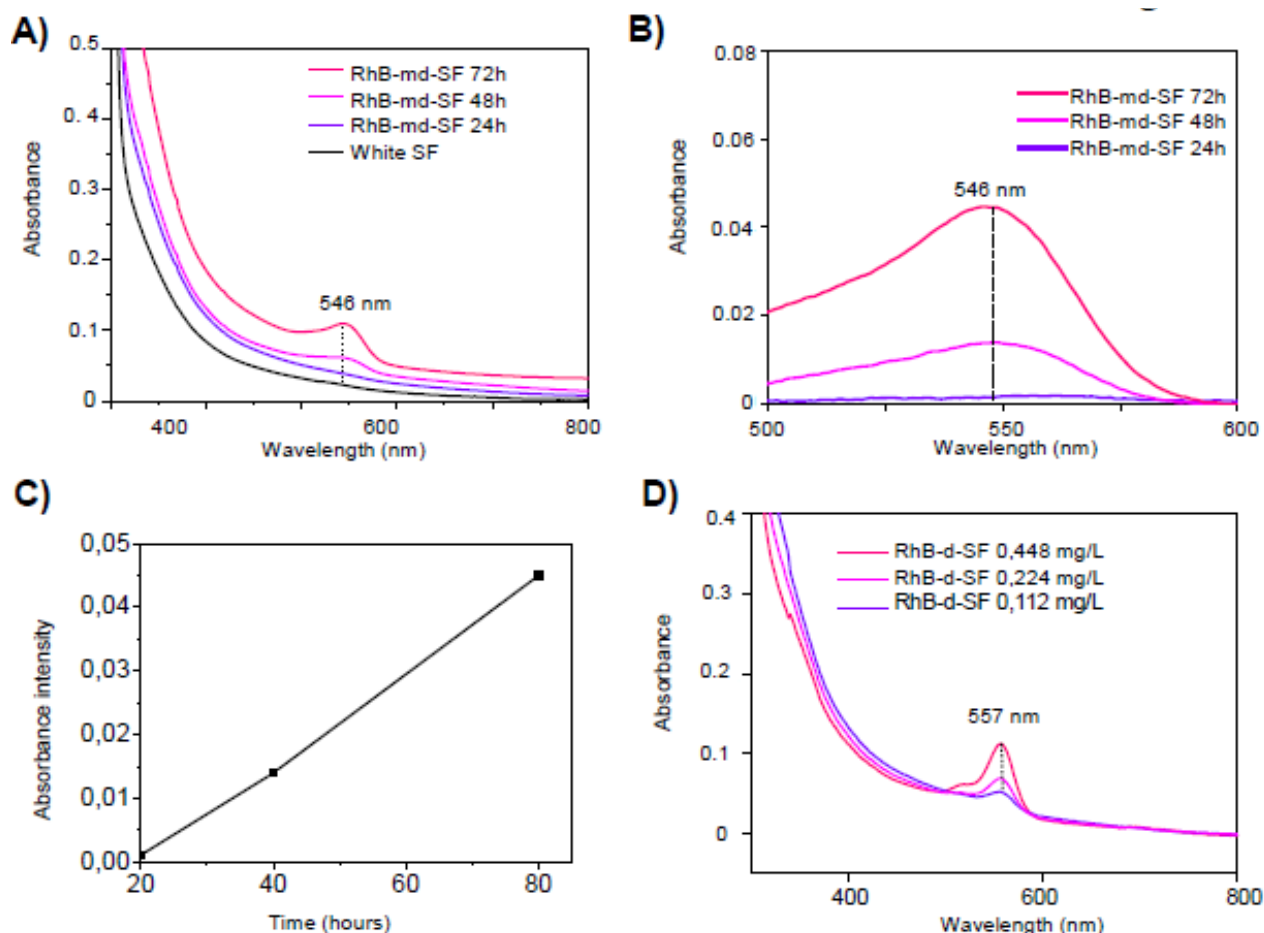
Figure 22. A-B) UV-VIS absorption spectra of RSF water-solutions collected in the 300–800 (A) and 450–650 nm regions (B). C) Maximal UV-VIS ABS values versus time (24, 48, 72 hours) of exposure of larvae to diet containing RhB. D) UV-VIS absorption spectra in the 300–800 nm region of RhB-doped SF (RhB-d-SF) at different concentrations of dye (0.448 mg L^{-1}; 0.224 mg L^{-1}; 0.112 mg L^{-1}).

RhB-md-SF and RhB-d-SF water-solutions were excited at 295 nm (figure 23A-B) and 325 nm (figure 23C-D) to evaluate the behaviour of the amino acid residues.[128] Upon excitation at 295 nm (figure 23A-B), all fluorescence spectra displayed a wide band at 350 nm, attributed to emission of Trp residues that are much more exposed to bulk water.[129,130] When RhB-md-SF solutions were excited at 325 nm (figure 23C-D), fluorescence spectra were characterized mainly by two features: a broad structured emission with maxima at 400 and 415 nm (typical of the singly ionized di-tyrosine chromophore and oxidized tryptophan)[131] and a peak at 568 nm of increasing intensity from RhB-md-SF 48h to RhB-md-SF 72h. The latter peak was almost undetectable in the RhB-md-SF 24h. When excited at 325 nm, the white SF fluorescence spectrum displayed only the two bands at 400 and 415 nm (figure 23C). The emission profiles of RhB-d-SF samples, recorded by exciting at

the same wavelength (325 nm), were comparable to those of natural coloured samples. Indeed, the broad band (400–415 nm) and the emission of dye were still present, although the latter was shifted from 568 nm to 575 nm (figure 23D). However, the presence of these species (di-tyrosine and oxidized tryptophan) in RSF water-solutions could be derived from the treatments that the protein chains are subjected to during the various phases of extraction and purification of fibroin from the cocoons.
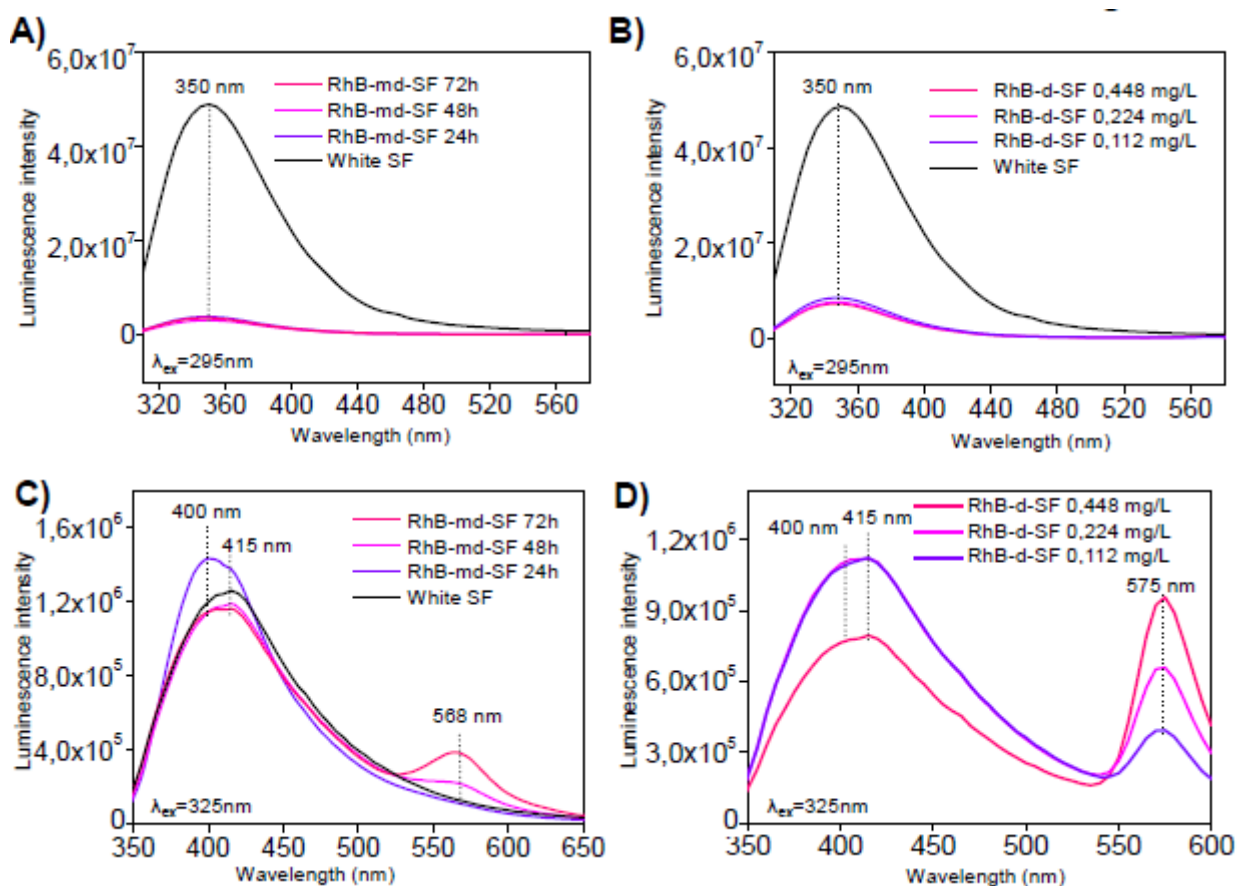
Figure 23. Emission profiles of white, natural coloured RSF water-solutions and RhB-doped SF solutions recorded by exciting at 295 nm (A-B) and 325 nm (C-D).

In order to examine the fluorescence features of RhB in the different systems, we excited the various solutions of RhB at 546 nm. In all cases, the spectra were recorded from 550 nm to 750 nm. When the RhB-md-SF solutions were excited at 546 nm (figure 24A), the fluorescence spectra displayed the maximum intensity at 568 nm. Similar to the UV-VIS absorption, the intensity of emission also increased from RhB-md-SF 24h to RhB-md-SF 72h. As expected, no emission was observed when exiting the SF water-solution at 546 nm. On other hand, RhB-doped SF (figure 24B) solutions displayed the maximum emissions at 573 nm. Fluorescence bands of RhB-d-SF solutions were of greater intensity than those of RhB-md-SF samples.
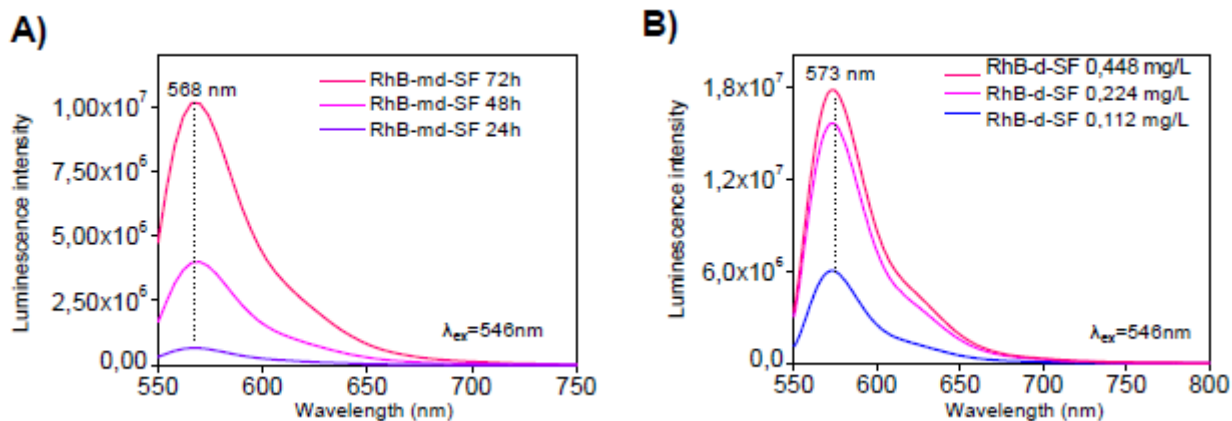
Figure 24. Emission profiles recorded by exciting at 546 nm natural coloured RSF water-solutions (A) and RhB-doped SF solutions (B).

Chemo-physical and conformational properties of the RSF films, realized by the DC approach, were investigated to verify their suitability for use as substrates in optical and photonic devices.

As shown in figure 25B, the SF films made by the white and RhB-md-SF 24h solutions were completely optically transparent (up to 95%) in the visible region (300–800 nm) with a clear consistent decrease under 277 nm as a result of protein absorbance. On the other hand, the RhB-md-SF 48h and RhB-md-SF 72h films showed a small loss in transparency around 550 nm, due to RhB absorption.

FT-IR analysis in the amide spectral regions (1200-1800 cm^{-1}) was performed to assign silk conformation to fibroin in silk films prepared by DC method from white and RhB-md-SF solutions (figure 25C). The IR spectra of all RhB-md samples does not show any relevant differences compared to the white SF films (figure 25C), indicating that the presence of RhB does not influence the self-assembling of fibroin chains during the film formation. The vibration peaks recorded for all SF samples were in agreement with the data previously described for films prepared by the same DC method, and confirm that SF film self-assembly properties were not modified by the diet-doping method.
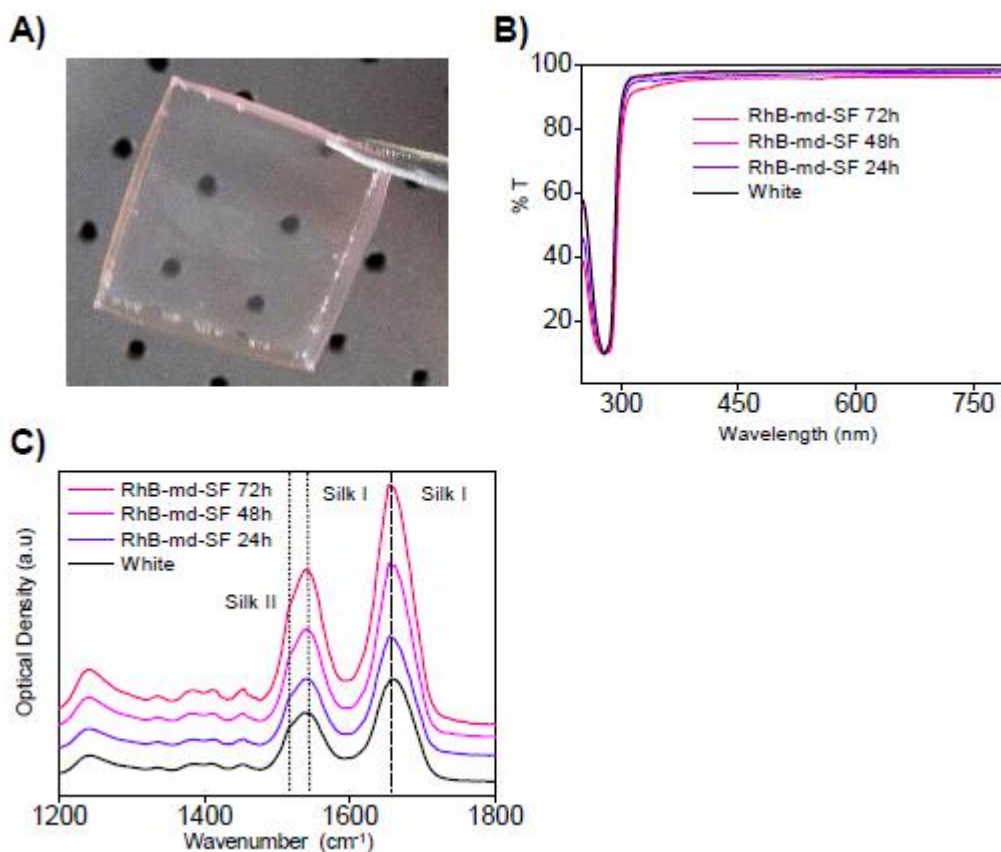
Figure 25. A) Natural coloured fibroin film obtained from RhB-md-SF 72h solution and prepared by DC method. B) Transmittance properties of white and natural coloured RSF films recorded from 250 to 800 nm. C) IR-FT spectra of white and natural coloured RSF films collected in the amide regions (1200–1800 cm^{-1}).

The same paradigm applied to SF solutions was used for all SF films in order to collect fluorescence profiles. By excitation at 325 nm and at 546 nm, we did not observe any difference in the spectral features of the RhB-md-SF solutions (figure 23C-D) and films (figure 26C-D). When exciting at 295 nm, we observed the emission of Trp residues at 330 nm, which some authors assigned to Trp residues enabled to give H-bonded exciplexes[130] (figure 26A). The fluorescence spectra of RhB-d-SF films were obtained also by excitation at 295 nm, 325 nm and 546 nm (figure 26B, 26D and 26F, respectively). The samples showed protein luminescence features comparable to those of RhB-md-SF films, in particular for the excitation at 295 nm where the peak at 330 nm appeared (figure 26B). On the other hand, the signal of the dye was different for the emission wavelength (573 nm instead of 568 nm) and the form of the curve (figure 26F). This could be associated with a different assembling or bonding of molecules when the RhB is dispersed in white SF solutions.
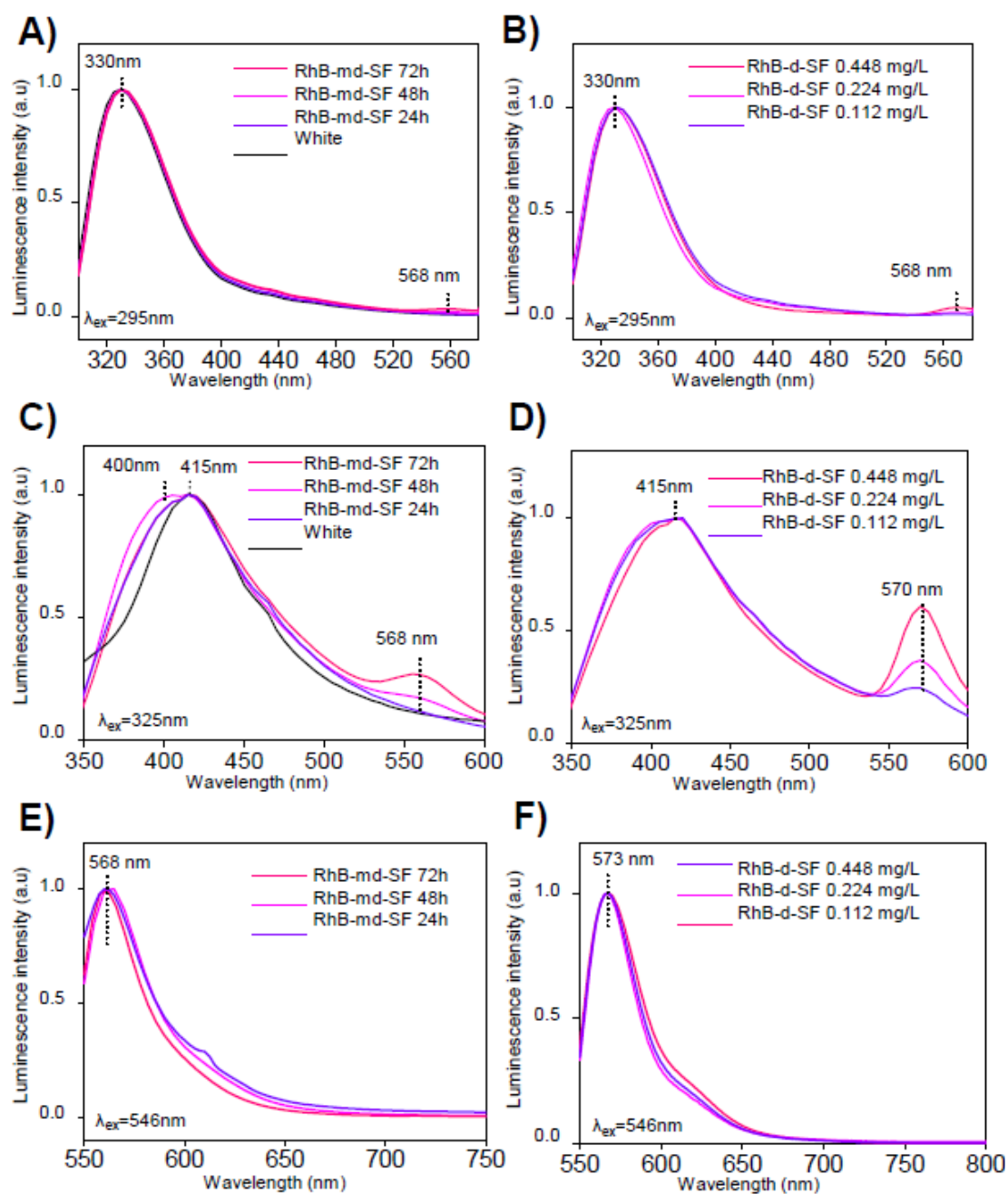
Figure 26. Emission profiles of fibroin films obtained from white, natural coloured SF and RhB doped SF solutions. The fluorescence spectra were recorded by exciting at: 295 nm (A and B), 325 nm (C and D), 546 nm (E and F). Fibroin films were prepared by the DC approach on quartz substrates.

This work demonstrated that biodoping method is suitable for the biomanufacturing of doped and optically active silk solutions and films. The RhB-md-SF solutions and films showed UV-VIS and fluorescent features typical for the presence of RhB. Moreover RhB-md-SF films were optically transparent and protein self-assembly properties were not modified.

4.4.2 Chemical functionalization of silk fibroin via silylation

SF contains serine, threonine, aspartic and glutamic acid, and tyrosine that can all be targeted and modified exploiting known organic synthesis procedures such as carbodiimide coupling or OH grafting.[132] On this line, here we report a novel approach for chemically modified SF even with hydrophobic molecules relying on the use of APTES, a common silylating agent exploited also for the formation of self-assembled monolayer,[133] which acts as solvent, carrier in water and grafting agent simultaneously. A fluorescent ester ended oligothiophene (T_3) was used as model hydrophobic system for monitoring the process trough fluorescence detection.

Synthesis of SF-APTES-T$_3$ composite. The proposed synthetic approach is depicted in figure 27A-B and widely described in Materials and Methods section. T_3 was dissolved in APTES (final conc. 0.025 M), this solution was sonicated and then added to RSF water-solution. As-made blend SF-APTES-T$_3$ solution was stirred for 1h on a tube rotator and finally purified by size exclusion chromatography (SEC, Sephadex G25 desalting column) by using DI water as eluent. Figure 26C shows the image of the elution under UV lamp illumination.

A single fluorescent band can be clearly distinguished along the column and no fluorescent residues at the column edge are observed. This evidence indicates the formation of a stable, water soluble SF-APTES-T$_3$ complex. Accordingly, when dichlorometane (CH_2Cl_2) was added to an eluted fraction, fluorescence was observed only in the water phase (figure 26D, right panel). In contrast to a control experiment, as shown by the figure 26E, the fluorescence of the APTES-T$_3$ adduct in absence of SF is observed in both water and organic phases (figure 26E, right panel).
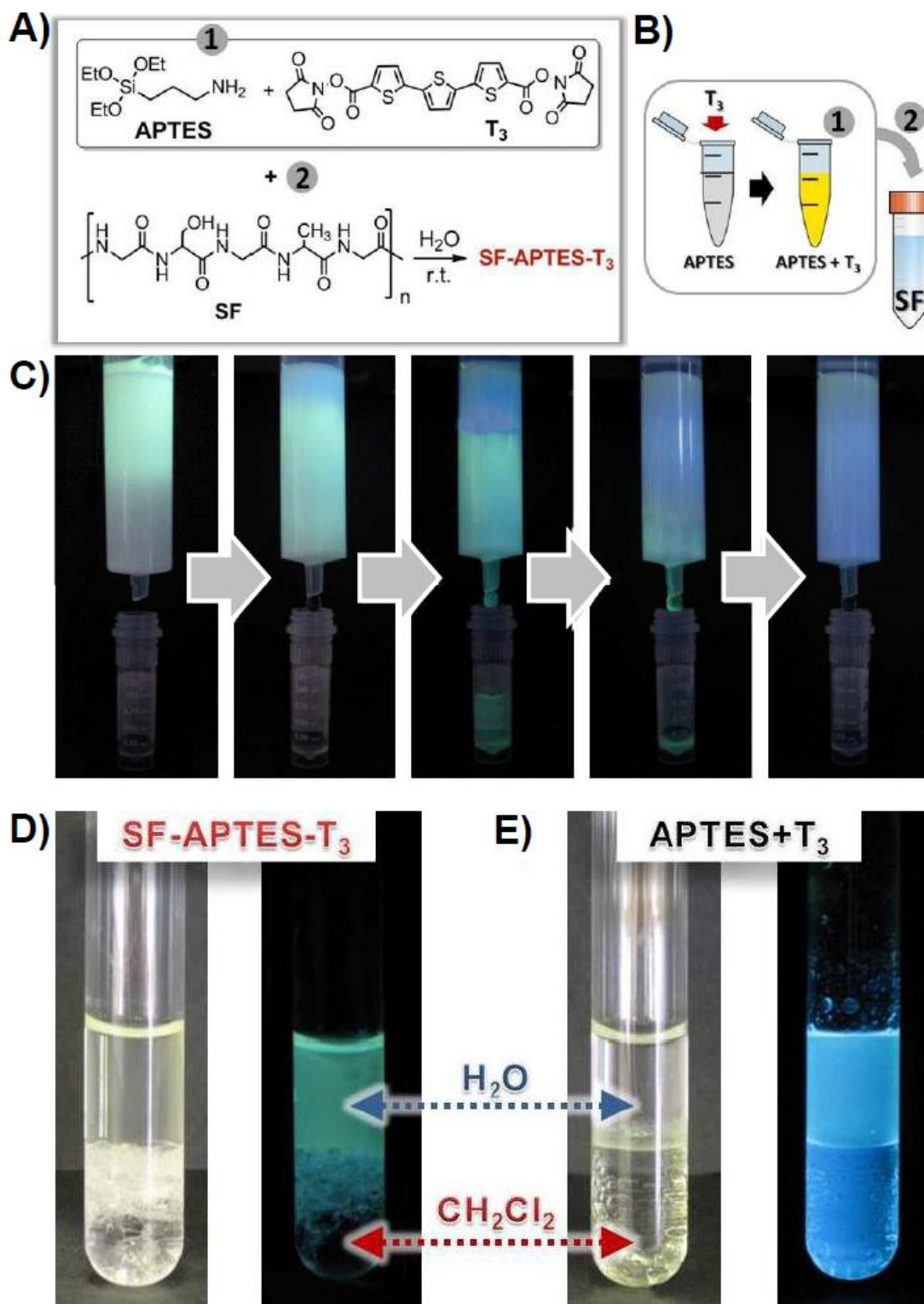
Figure 26. A) synthetic route for APTES mediated SF chemical modification and B) sketch of the procedure. C) Image under UV illumination of the elution of SF-APTES-T_3 through SEC by using water as eluent. D) SF-APTES-T_3 in water after addition of CH_2Cl_2, the fluorescence remains in the water phase. E) T_3 dissolved in APTES after addition of CH_2Cl_2 and water, fluorescence is observed from both phases.

Chemo-physical properties of SF-APTES-T3 composite. The possibility of covalent bond formation through APTES promoted silylation[134] of SF hydroxyl residues was investigated by ^{1}H-NMR experiments[135] in comparison to unmodified SF. A SEC eluted fraction (figure 27A) of SF-APTES-T_3 (1 mL) was casted on PDMS flat surface and dried to give a free-standing SF-APTES-T_3 film (figure 27B-C) that was then dissolved in D_2O. The spectrum (figure 27D) shows the same fingerprint of unmodified SF (figure 27E) and the signals of the CH_2 groups of APTES (marked with asterisks in figure 27D) that appeared as resolved and sharp signals, this suggesting that APTES (hydrolytically unstable, in water $t_{1/2}$ = 8h at 25°C, pH 7) did not polymerize neither after slow dehydration.
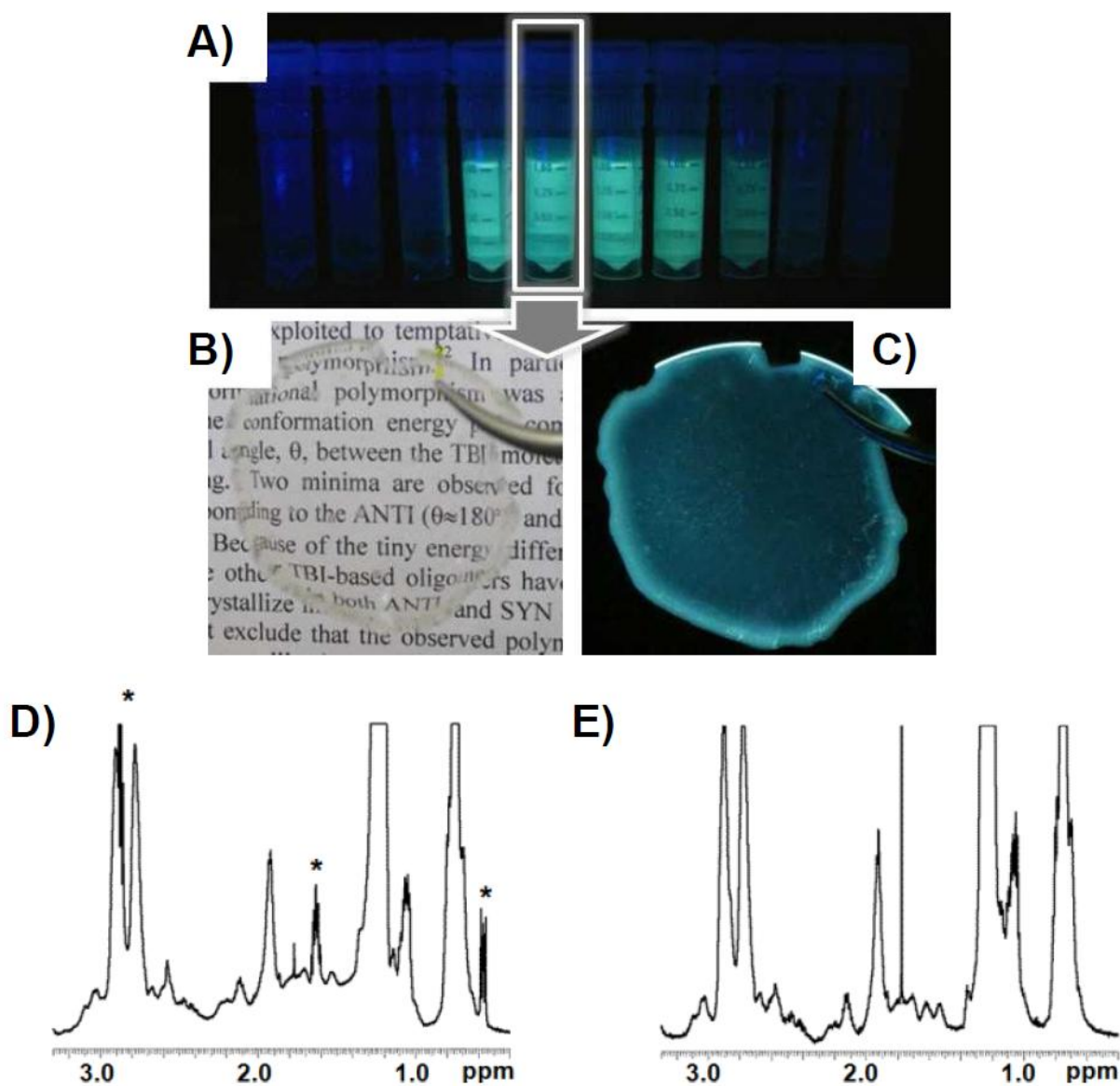
Figure 27. A) images under UV lamp illumination of the fractions eluted by SEC. B-C) SF-APTES-T_3 free-standing film under normal (B) and UV (C) light illumination. D) ^{1}H-NMR spectrum of SF-APTES-T_3 film portion dissolved in D_2O and E) spectrum of SF film under the same experimental conditions. Asterisks in spectrum D) indicate the CH_2 signals of APTES.

Interestingly, the SF-APTES-T_3 film (figure 28A, orange curve) preserved the same optical transparency of pure SF film (black line) in visible range. Photoluminescence spectra of the new silk composite solution and film are shown in figure 28B. A blue greenish fluorescence was observed by emission spectroscopy (figure 28B, orange curve) and ascribed to the T_3 moiety, as confirmed by the overlap with the PL spectrum of T_3 in SF-APTES water-solution (figure 28B, blue curve).

ATR FT-IR) was performed to investigate SF secondary structures in SF-APTES-T_3 film (figure 28C). In the amide I region, spectra of SF and SF-APTES-T_3 samples show typical vibration peaks attributed to silk I conformation (random coils/extended chains) between 1640-1645 cm^{-1}. In amide II region, spectra of SF and SF-APTES-T_3 show the same peak of silk I conformation at 1538 cm^{-1} but a strong shift to 1517 cm^{-1} (silk II) is observed for SF-APTES-T_3. In amide III region, a peak at 1233 cm^{-1} of silk II conformation is observed only for SF-APTES-T_3. Therefore collectively, ATR spectroscopy shows that APTES-T_3 does not change self-assembling of fibroin, indeed infrared spectra are overlapping in amide regions; a small conformational change (in amide II and III regions) is observed for SF-APTES-T_3. Interestingly, spectrum (figure 28D) of SF films doped by T_3 dissolved in DMSO and prepared under the same conditions display vibration properties of silk II conformation due to β-sheet secondary structures (1623 cm^{-1} and 1700 cm^{-1}). Collectively these results indicated that SF-APTES-T_3 is not altering the SF β-sheet contents and secondary structures, while SF doped with DMSO (used as solvent for adding T_3 to RSF water-solution at the same %v/v) affects SF conformational properties.
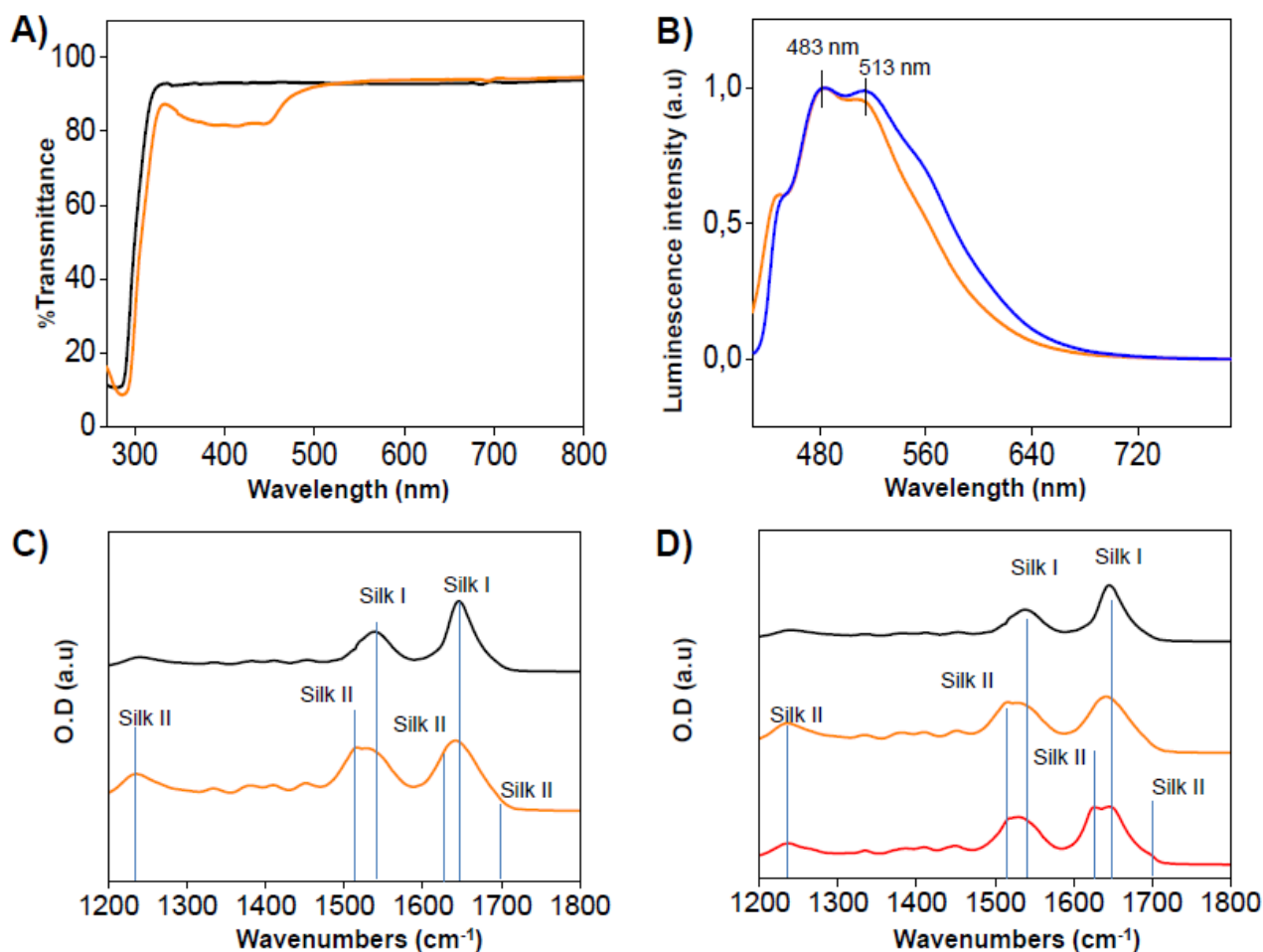
Figure 28. A) Optical transparency of SF-APTES-T_3 (orange curve) and SF (black curve) films. B) Emission spectra of SF-APTES-T_3 film (orange curves) and of T_3 in SF-APTES water-solution at the same concentration (blue curve). λ_{exc} = 400 nm. C) ATR FT-IR spectra of SF (black curve) and SF-APTES-T_3 (orange curve) films. D) The same spectra are reported together to ATR FT-IR spectrum of a silk film obtained from DMSO-T_3 doped SF solution (red line). All silk films were made by the same DC method.

Finally, stress-strain mechanical tests were carried out to study the mechanical properties of SF-APTES-T_3 composite. Table 5 shows that the Young's modulus and the Ultimate Tensile Strength (UTS) of SF-APTES-T_3 increase with respect to those of SF (30% and 60% increase, respectively), confirming a cooperative intermolecular interaction between SF chains due to APTES-T_3. As result of this cooperation SF chains are packed tightly, resulting in an increase of rigidity of the composite.

	E/ Nmm^{-2}	F max/Nmm^{-2}	ε/%
SF	2433 ± 72	33.5 ± 9.6	1.8±0.2
SF-APTES-T$_3$	3169 ± 83	53.5 ± 9.7	2.1±0.3

Table 5. Mechanical Properties of SF-APTES-T$_3$ with respect to SF.

In conclusion, we have reported a method for chemically modifying *B. mori* regenerated SF based on the use of APTES which acts as a bifunctional linker of an hydrophobic molecule, solvent and reinforcing agent simultaneously. Remarkably, SF-APTES-T$_3$ shows synergetic filmability and transparency of silk, combined with enhanced robustness imparted by APTES and fluorescence properties of T$_3$. These results highlight the potential of the proposed approach for fabricating multifunctional SF-APTES biocomposites grafted by any other hydrophobic molecule such as fluorescent dyes and drugs.

5. Conclusions

The results obtained during my PhD research activity confirmed that silk fibroin is a versatile biomaterial that can be prepared in various silk-based forms. In particular, we standardized production, extraction and purification of regenerated silk film, to control its chemo-physical properties, biocompatibility, mechanical and biodegradation behaviour to respond the demand for innovation in biomedical application and pharmaceutical formulations.

In this context we also identified different methods and approaches to tailor and improve features of pure silk films to target and broad its exploitation possibilities. The novel synthesized and fabricated silk fibroin nanocomposites displayed synergy effect with improved properties with respect to the single component in terms of mechanical strength, resistance to biodegradation, biocompatibility.

We also designed and optimized chemical strategies to obtain silk fibroin composite. Two step water based chemical modification via silylation was demonstrated to be suitable for obtaining silk-sililated film substrates with define chemo-physical features. Finally, we demonstrated that the process to fabricate doped silk film by taking advantage of cocoon chemical factory can be realized, controlled and optimized for biomedical and pharmaceutical application. Because of the large-scale

cultivation of silkworms for the textile industry, there are abundant and reasonable sources for this natural polymer. Applicability of the proposed concepts and optimized methods obtained from the results of my PhD thesis could set the scene for the use of silk as innovative technological substrates and encourage application, ideas and research avenues that follow greener methods for sustainable chemistry in biopharmaceutical applications. However, process up-scale, that would determine exploitation and attractiveness for industrial application is still challenging and would require further development of the presented results in future studies.

6. Pubblication list

*Results will refer to the topics described above and will include mainly the following reference list.

1. Bonetti S., Pistone A., Brucale M., Karges S., Favaretto L., Zambianchi M., Posati T., **Sagnella A.**, Caprini M., Toffanin S., Zamboni R., Camaioni N., Muccini M., Melucci M., Benfenati V."*A Lysinated thiophene based semiconductor as a multifunctional neural bioorganic interface*", Advanced Healthcare Materials in press.

2. Cavallini S., Toffanin S., Chieco C., **Sagnella A.**, Formaggio F., Pistone A., Posati T., Natali M., Caprini M., Benfenati V., Di Virgilio N., Ruani G., Muccini M., Zamboni R.,Rossi F., *Naturally functionalized silk as useful material for photonic applications*, Composites Part B 2015, 71, 152.

3. **Sagnella A.**, Chieco C., Benfenati V., Di Virgilio N., Toffanin S., Cavallini S., Posati T., Pistone A., Varchi G., Bonetti S., Ruani G., Muccini M., Rossi F., Zamboni R., *SILK.IT project: Silk Italian Technology for industrial biomanufacturing,* Composites Part B 2015, 68, 281.

4. **Sagnella A.**, Chieco C., Di Virgilio N., Toffanin S., Posati T., Pistone A., Bonetti S., Muccini M., Ruani G., Benfenati V., Rossi F., Zamboni R. *Bio-doping of regenerated silk fibroin solution and films: a green route for biomanufacturing,* RSC Advances 2014, 4, 33687.

5. Posati T., Benfenati V., **Sagnella A.**, Pistone A., Nocchetti M., Donnadio A., Ruani G., Zamboni R., Muccini M. *Innovative Multifunctional Silk Fibroin and Hydrotalcite Nanocomposites: A Synergic Effect of the Components,* Biomacromolecules 2014, 15, 158.

6. Posati T., Melucci M., Benfenati V., Durso M., Nocchetti M., Cavallini S., Toffanin S., **Sagnella A.**, Pistone A., Muccini M., Ruani G., Zamboni R., *Selective MW-assisted surface chemical tailoring of hydrotalcites for fluorescent and biocompatible nanocomposites,* RSC Advances 2014, 4, 11840.

7. Dionigi C., Posati T., Benfenati V., **Sagnella A.**, Pistone A., Bonetti S., Ruani G., Dinelli F., Padeletti G., Zamboni R., Muccini M. *Nanostructured conductive bio-composite of silk fibroin/single walled carbon nanotube,* Journal of Materials Chemistry B 2014, 2, 1424.

8. Toffanin S., Benfenati V., Pistone A., Bonetti S., Koopman W., Posati T., **Sagnella A.**, Natali M., Zamboni R., Ruani G., Muccini M. *N-type perylene-based organic semiconductors for functional neural interfacing,* Journal of Materials Chemistry B, 2013, 1, 3850.

9. .Benfenati V., Toffanin S., Bonetti S., Turatti G., Pistone A., Chiappalone M., **Sagnella A.**, Stefani A., Generali G., Ruani G., Saguatti D., Zamboni R., Muccini M. *A transparent organic transistor structure for bidirectional stimulation and recording of primary neurons,* Nature Materials, 2013, 12, 672.

10. Melucci M., Durso M., Favaretto L., Capobianco M. L., Benfenati V., **Sagnella A.**, Ruani G., Muccini M., Zamboni R., Fattori V., Nadia C. *Silk doped with a bio-modified dye as a viable platform for eco-friendly luminescent solar concentrators*, RSC Advances, 2012, 2, 8610.

11. .Benfenati V., **Sagnella A.**, Chieco C., Di Virgilio N., Muccini M., Zamboni R., Rossi F. *Silk fibroin as platform for neural cells and hybrid optoelectronics*, Journal of Biobased Materials and Bioenergy 2012, 6, 508.

12. Ambrogi V., Perioli L., Pagano C., Marmottini F., Ricci M., **Sagnella A.**, Rossi C. *Use of SBA-15 for furosemide oral delivery enahancement,* European journal of Pharmaceutical Science 2012, 46, 43.

13. .Benfenati V., Sthal K., Gomis-Perez C., Toffanin S., **Sagnella A.**, Torp R., Kaplan D.L., Omenetto F.G., Zamboni R., Muccini M. *Biofunctional Silk/Neuron Interfaces,* Advanced Functional Materials 2012, 22, 1871.

7. Acknowledgement

First I would to thank my co-supervisor Valentina Benfenati. I appreciated all her contributions of time and ideas. She stimulated to improve my scientific and productive experience. The joy and enthusiasm she has for her research was contagious and motivational for me. My colleagues Tamara Posati, Assunta Pistone, Simone Bonetti, Emanuela Saracino, Saskia Kerges, Ana Borrachero and Francesco Formaggio, that are the members of the Benfenati group. They have contributed immensely to my personal and professional growth. The group has been a source of friendships as well as good advices and collaborations. I am especially grateful to Tamara Posati and Assunta Pistone who were the first people that start with me this research work experience in Benfenati

8. References

1. C. P. Bergmann and A. Stumpf, *Dental Ceramics, Topics in Mining, Metallurgy and Materials Engineering*, Springer-Verlag Berlin Heidelberg 2013, DOI: 10.1007/978-3-642-38224-6_2.

2. L. A. Pruitt and A. M. Chakravartula, *Mechanism of Biomaterials- Fundamental and Principles for Implant Design*, Cambridge University press New York 2011.

3. N. R. Patel, P. P. Gohil, *A review on biomaterials: scope, applications & human anatomy significance*, IJETAE 2012, 2, 91-101.

4. B. D. Ulery, L. S. Nair, C. T. Laurencin, *Biomedical applications of biodegradable polymers*, J Polym Sci B: Polym Phys 2011, 49, 832–864.

5. E. Marin, M. I. Briceño, C. Caballero-George, *Critical evaluation of biodegradable polymers used in nanodrugs,* Int J Nanomedicine 2013, 8, 3071-3091.

6. I. Vroman, L. Tighzert, *Biodegradable polymers*, Materials 2009, 2, 307–344.

7. I. C. Celerino de Moraes Porto, *Polymer Biocompatibility*, INTECH Chapter 3, 2013, http://dx.doi.org/10.5772/47786.

8. E. Hassan, Y. Wei, H. Jiao, Y. Muhuo, *Dynamic Mechanical Properties and Thermal Stability of Poly(lactic acid) and Poly(butylene succinate)Blends Composites,* JFBI 2013, 6, 85-94.

9. J.-F. Larché, P.-O. Bussière, S. Thérias, J.-L. Gardette, *Photooxidation of polymers: Relating material properties to chemical changes,* Polym Degrad Stabil 2012, 97, 25-34.

10. B. A. Miller-Chou, J. L. Koenig, *A review of polymer dissolution,* Prog Polym Sci 2003, 28, 1223–1270.

11. I. J. Ogaji, E. I. Nep, J. D. Audu-Peter, *Advances in Natural Polymers as Pharmaceutical Excipients*, Pharm Anal Acta 2012, 3, 146. doi:10.4172/2153- 2435.1000146.
12. V. Pillay, A. Seedat, Y. E. Choonara, L. C. du Toit, P. Kumar, V. M. K. Ndesendo, *A Review of Polymeric Refabrication Techniques to Modify Polymer Properties for Biomedical and Drug Delivery Application,* AAPS Pharm Sci Tech 2013, 14, 692-711.

13. V. Benfenati, S. Toffanin, R. Capelli, L. M. A. Camassa, S. Ferroni, D. L. Kaplan, F. G. Omenetto, M. Muccini, R. Zamboni, *A silk platform that enables electrophysiology and targeted drug delivery in brain astroglial cells,* Biomaterials 2010, 31, 7883−7891.

14. V. Benfenati, K. Stahl, C. Gomis-Perez, S. Toffanin, A. Sagnella, R. Torp, D. L. Kaplan, G. Ruani, F. G. Omenetto, R. Zamboni, M. Muccini, *Biofunctional Silk/Neuron Interfaces,* Adv Funct Mater 2012, 22, 1−14.

15. V. Benfenati, S. Toffanin, S. Bonetti, G. Turatti, A. Pistone, M. Chiappalone, A. Sagnella, A. Stefani, G. Generali, G. Ruani, D. Saguatti, R. Zamboni, M. Muccini, *A transparent organic transistor structure for bidirectional stimulation and recording of primary neurons,* Nat Mater, 2013, 12, 672-81.

16. M. H. Mohammed, P. A. Williams, O. Tverezovskaya, *Extraction of chitin from prawn shells and conversion to low molecular mass chitosan,* Food Hydrocolloid 2013, 31, 166–171.

17. I. Younes, O. Ghorbel-Bellaaj, R. Nasri, M. Chaabouni, M. Rinaudo, M. Nasri, *Chitin and chitosan preparation from shrimp shells using optimized enzymatic deproteinization,* Process Biochem 2012, 47, 2032-2039.

18. C. K. S. Pillai, W. Paul, C. P. Sharma, *Chitin and chitosan polymers: Chemistry, solubility and fiber formation,* Prog Polym Sci 2009, 34, 641–678.

19. H. Fredriksson, J. Silverio, R. Andersson, A. C. Eliasson, P. Aman, *The influence of amylase and amylopectine characteristics on gelatinization and retrogradation properties of different starches*, Carbohyd Polym 1998, 35, 119-134.

20. W. S. Ratnayake, R. Hoover, F. Shahidi, C. Perera, J. Jane, *Composition, molecular structure and physicochemical properties of starches from four field pea cultivars,* Food Chem 2001, 74, 189-202.

21. A. N. Netravali, S. Chabba, *Composites get greener*, Mat Today 2003, 6, 22-29.

22. S. M. Parandoosh, S. M. Hudson, *The acetylation and enzymatic degradation of starch films*, J Appl Polym Sci 1993, 48, 787-791.

23. J. W. Lawton, G. F. Fanta, *Glycerol-plasticized films prepared from starch-poly(vinyl alcohol) mixture : effect of poly(ethylene-co-acrylic acid)*, Carbohyd Polym 1994, 23, 275-280**.**

24. X. Wang, K. Yang, Y. Wang, *Properties of starch blends with biodegradable polymers*, J. Macrom Sci C-Polym Rev 2003, 43, 385-409.

25. R. Chandra, R. Rustgi, *Biodegradable polymers,* Progr Polym Sci 1998, 23, 1273-1335.

26. J. D.Gu, D. Eberiel, S. P. McCarthy, R. A. Gross, *Cellulose acetate biodegradability upon exposure to simulated aerobic composting and anaerobic bioreactor environments,* J Environ Polym Degr 1993, 1, 143-153.

27. J. D. Gu, D. Eberiel, S. P. McCarthy, R. A. Gross, *Degradation and mineralization of cellulose*

acetate in simulated thermophilic compost environments, J Environ Polym Degr 1993, 1, 281-291.

28. A. D. Augst, H. J. Kong, D. J. Mooney, *Alginate hydrogels as biomaterials,* Macromol Biosci. 2006, 6, 623-33.

29. L. Robert, *Hyaluronan, a truly "youthful" polysaccharide. Its medical applications,* Pathol Biol 2014, IN PRESS

30. L. Robert, A. M. Robert, G. Renard, *Biological effects of hyaluronan in connective tissues, eye, skin, venous wall. Role in aging,* Pathol Biol 2010, 58, 187–98.

31. E. A. Balazs, M. Hargittai, I. Hargittai, *Hyaluronan. From basic science to clinical applications,* Edgewater (NJ) PubMatrix 2011 [Vols 1 to 5].

32. X. Hu, P. Cebe, A. S. Weiss, F. Omenetto, D. L. Kaplan, *Protein-based composite materials,* Mater Today 2012, 15, 208-215.

33. T. R. Cuya Guizado, *Analysis of the structure and dynamics of human serum albumin*, J Mol Model 2014, 20, 2450-2463.

34. F. Wong, *Drug insight: the role of albumin in the management of chronic liver disease*, Nat Clin Pract Gastroenterol Hepatol 2007,4,43–51.

35. F. Kratz, *A clinical update of using albumin as a drug vehicle — A commentary,* J Control Release 2014, 190, 331–336.

36. C. Bertucci, A. De Simone, M. Pistolozzi, M. Rosini, *Reversible Human Serum Albumin Binding of Lipocrine: A Circular Dichroism Study,* Chyrality 2011, 23, 827–832.

37. T. R. C. Guizado, S. R.W. Louro, C. Anteneodo, *Dynamics of heme complexed with human serum albumin: a theoretical approach*, Eur Biophys J 2012, 41, 1033–1042.

38. R. P. Bareil, R. Gauvin, F. Berthod, *Collagen-Based Biomaterials for Tissue Engineering Applications,* Materials 2010, 3, 1863-1887.

39. L. Cen, W. Liu, L. Cui, W. Zhang, Y. Cao, *Collagen Tissue Engineering: Development of Novel Biomaterials and Applications,* Pediatr Res 2008, 63, 492-496.

40. M. Kikuchi, *Hydroxyapatite/Collagen Bone-Like Nanocomposite*, Biol Pharm Bull 2013, 36, 1666–1669.

41. M. C.Gomez-Guillen, M. Perez-Mateos, J. Gomez-Estaca, E. Lopez-Caballero, B. Gimenez, P. Montero, *Fish gelatin: A renewable material for developing active biodegradable films,* Trends Food Sci Technol 2009, 20, 3-16.

42. N. Cao, X. Yang, Y. Fu, *Effetcs of various plasticizers on mechanical and water vapor barrier properties of gelatin films*, Food Hydrocoll 2009, 23, 729-735.

43. H. H. Bragulla, D. G. Homberger, *Structure and functions of keratin proteins in simple, stratified, keratinized and cornified epithelia,* J Anat 2009, 214, 516–559.

44. B. Srinivasan, R. Kumar, K. Shanmugam, U. T. Sivagnam, N. P. Reddy, P. K. Sehgal, *Porous keratin scaffold–promising biomaterial for tissue engineering and drug delivery*, J Biomed Mater Res Part B 2010, 92, 5-12.

45. B. Kundu, N. E. Kurland, S. Bano, C. Patra, F. B. Engel, V. K. Yadavalli, S. C. Kundu, *Silk proteins for biomedical applications: Bioengineering perspectives*, Prog Polym Sci 2014, 39, 251–267.

46. D. N. Rockwood, R. C. Preda, T. Yücel, X. Wang, M. L. Lovett, D. L. Kaplan, *Materials fabrication from Bombyx mori silk fibroin*, Nat Protoc 2011, 6, 1612-1631.

47. R. Lewis, *Unraveling the weave of spider silk*, Bioscence 1996, 46, 636-638**.**

48. M. Mondal, K. Trivedy, S. Nirmal Kumar, *The silk proteins, sericin and fibroin in silkworm, Bombyx mori Linn., - a review* Caspian J Env Sci 2007, 5, 63-76.

49. K. Tanaka, N. Kajiyama, K. Ishikura, S. Waga, A. Kikuchi, K. Ohtomo, T. Takagi, S. Mizuno, *Determination of the site of disulfide linkage between heavy and light chains of silk fibroin produced by Bombyx mori*, Biochim Biophys Acta Protein Struct Mol Enzymol 1999, 1432, 92-103.

50. T. Yucel, M. L. Lovett, D. L. Kaplan, *Silk-based biomaterials for sustained drug delivery*, J Control Release 2014, 190, 381–397.

51. K. S. Hossain, A. Ochi, E. Ooyama, J. Magoshi, N. Nemoto, *Dynamic lights scattering of Native Silk Fibroin solution extracted from different parts of the middle division of the silk gland of the Bombyx mori silkworm*, Biomacromolecules 2003, 4, 350-359.

52. T. Gamo, T. Inocukhi, H. Laufer, *Polypeptides of fibroin and sericin secreted from the different sections of the silk gland in Bombyx mori,* Insect Biochem 1977, 7, 285-295.

53. Y. Tashiro, E. Otsuki, *Studies on the posterior silk gland of the silkworm Bombyx mori. Ultracentrifugal analyses of native silk proteins, especially fibroin extracted from the middle silk gland of the mature silkworm,* J Cell Biol 1970, 46, 1-16.

54. M. Yang, Y. Shuai, W. He, S. Min, L. Zhu, *Preparation of porous scaffolds from silk fibroin extracted from the silk gland of Bombyx mori (B. mori),* Int J Mol Sci 2012, 13, 7762-7775.

55. H. Wang, Y. Zhang, H. Shao, X. Hu, *A study on the flow stability of regenerated silk fibroin aqueous solution,* Int J Biol Macromol. 2005, 36, 66-70.

56. A. Matsumoto, J. Chen, A. L. Collette, U.-J. Kim, G. H. Altman, P. Cebe, D. L. Kaplan**,** *Mechanisms of silk fibroin sol−gel transitions,* J Phys Chem B 2006, 110, 21630–38.

57. J. Nam, Y. H. Park, *Morphology of regenerated silk fibroin: effects of freezing temperature, alcohol addition, and molecular weight,* J Appl Polym Sci 2001, 81, 3008–302.

58. C.-Z. Zhou, F. Confalonieri, M. Jacquet, R. Perasso, Z.-G. Li, J. Janin, *Silk fibroin: structural implications of a remarkable amino acid sequence,* Proteins Struct Funct Bioinform 2001, 44, 119–122.

59. H.J. Jin, D.L. Kaplan, *Mechanism of silk processing in insects and spiders*, Nature 2003, 424, 1057–1061.

60. H. J. Jin, J. Park, V. Karageorgoiu, U.J. Kim, R. Valluzzi, P. Cebe, D.L. Kaplan *Water-stable silk films with reduced β-sheet content,* Adv Funct Mater 2005, 15, 1241-1247.

61. A. S. Lammel, X. Hu, S.-H. Park, D. L. Kaplan, T. R. Scheibel, *Controlling silk fibroin particle features for drug delivery,* Biomaterials 2010, 31, 4583-4591.

62. B. D. Lawrence, F. Omenetto, K. Chui, D. L. Kaplan, *Processing methods to control silk fibroin film biomaterial features,* J Mater Sci 2008, 43, 6967–6985.

63. T. Yucel, P. Cebe, D.L. Kaplan, *Vortex-induced injectable silk fibroin hydrogels,* Biophys J 2009, 97, 2044–2050**.**

64. G.G. Leisk, T.J. Lo, T. Yucel, Q. Lu, D.L. Kaplan, *Electrogelation for protein adhesives,* Adv Mater 2010, 22, 711–715.

65. T. Asakura, Y. Suzuki, Y. Nakazawa, G. P. Holland, J. L. Yarger, *Elucidating silk structure using solid-state NMR*, Soft Matter 2013, 9,11440–11450.

66. R. E. Marsh, R. B. Corey, L. Pauling, *An investigation of the structure of silk fibroin*, Biochim Biophys Acta 1955, 16, 1–34.

67. R. Valluzzi, S. P. Gido, W. Muller, D. L. Kaplan, *Orientation of silk III at the air–water interface*, Int J Biol Macromol 1999, 24, 237–242.

68. B. Kundu, R. Rajkhowa, S. C. Kundu, X. Wang, *Silk fibroin biomaterials for tissue regenerations,* Adv Drug Deliv Rev 2013, 65, 457-470.

69. H. Tao, M. A. Brenckle, M. Yang, J. Zhang, M. Liu, S. M. Siebert, R. D. Averitt, M. S. Mannoor, M. C. McAlpine, J. A. Rogers, D. L. Kaplan, F. G. Omenetto, *Silk-based conformal, adhesive, edible food sensors,* Adv Mater 2012, 24, 1067–1072.

70. E. Wenk, H. P. Merkle, L. Meinel, *Silk fibroin as a vehicle for drug delivery applications,* J Control Release 2011, 150, 128-141.

71. S. Sofia, M. B. McCarthy, G. Gronowicz, D. L. Kaplan, *Functionalized silk-based biomaterials for bone formation,* J Biomed Mater Res 2001, 54, 139–148.

72. Y. Gotoh, M. Tsukada, N. Minoura, Y. Imai, *Synthesis of poly(ethylene glycol)-silk fibroin conjugates and surface interaction between L-929 cells and the conjugates*, Biomaterials 1997, 18, 267–271.

73. A. R. Murphy, P. St John, D. L. Kaplan, *Modification of silk fibroin using diazonium coupling chemistry and the effects on hMSC proliferation and differentiation*, Biomaterials 2008, 19, 2829–2838.

74. N. Kasoju, U. Bora, *Silk fibroin in tissue engineering,* Adv Healthcare Mater, 2012*,* 1, 393–412.

75. D.-H. Kim, Y.-S. Kim, J. Amsden, B. Panilaitis, D. L. Kaplan, F. G. Omenetto, M. R. Zakin, J. A. Rogers, *Silicon electronics on silk as a path to bioresorbable, implantable devices,* Appl Phys Lett 2009, 95, 133701-3

76. K. McGrath, D. L. Kaplan, Eds.; *Protein-Based Materials;* Birkhauser Press: Boston, MA, 1996, 103-133.

77. H. Tao, D. L. Kaplan, F. G. Omenetto, *Silk Materials – A Road to Sustainable High Technology,* Adv Mater 2012, 24, 2824-2837.

78. C. Jiang, X. Wang, R. Gunawidjaja, Y.-H. Lin, M. K. Gupta, D. L. Kaplan, R. R. Naik, V. V. Tsukruk, *Mechanical properties of robust ultrathin silk fibroin films,* Adv Funct Mater 2007, 17, 2229–2237.

79. T. Posati, V. Benfenati, A. Sagnella, A. Pistone, M. Nocchetti, A. Donnadio, G.Ruani, R. Zamboni, M. Muccini, *Innovative multifunctional silk fibroin and hydrotalcite nanocomposites: a synergic effect of the components,* Biomacromolecules 2014, 15, 158−168.

80. A Sagnella, C. Chieco, N. Di Virgilio, S. Toffanin, T. Posati, A. Pistone, S. Bonetti, M. Muccini, G. Ruani, V. Benfenati, F. Rossi, R. Zamboni, *Bio-doping of regenerated silk fibroin solution and films: a green route for biomanufacturing,* RSC Adv 2014, 4, 33687–33694.

81. M. Prosa, A. Sagnella, T. Posati, M. Tessarolo, M. Bolognesi, S. Cavallini, S. Toffanin, V. Benfenati, M. Seri, G. Ruani, M. Muccini, Roberto Zamboni, *Integration of a silk fibroin based film as a luminescent down-shifting layer in ITO-free organic solar cells,* RSC Adv 2014, 4, 44815–44822.

82. C.-H. Wang, C.-Y. Hsieh, J.-C. Hwang, *Flexible organic thin-film transistors with silk fibroin as the gate dielectric*, Adv Mater 2011, 23, 1630–1634.

83. R. Capelli, J. J. Amsden, G. Generali, S. Toffanin, V. Benfenati, M. Muccini, D. L. Kaplan, F. G. Omenetto, R. Zamboni, *Integration of silk protein in organic and light-emitting transistors,* Org Electron 2011, 12, 1146–1151.

84. S. Toffanin, S. Kim, S. Cavallini, M. Natali, V. Benfenati, J. J. Amsden, D. L. Kaplan, R. Zamboni, M. Muccini, F. G. Omenetto, *Low-threshold blue lasing from silk fibroin thin films,* Appl Phys Lett 2012, 101, 091110-4.

85. A. Sagnella, C. Chieco, V. Benfenati, N. Di Virgilio, S. Toffanin, S. Cavallini, T. Posati, A. Pistone, G. Varchi, G. Ruani, M. Muccini, F. Rossi, R. Zamboni, *SILK.IT project: Silk Italian Technology for industrial biomanufacturing*, JCOMB 2015, 68, 281-7.

86. S. Cavallini, S. Toffanin, C. Chieco, A. Sagnella, F. Formaggio, A. Pistone, T. Posati, M. Natali, M. Caprini, V. Benfenati, N. Di Virgilio, G. Ruani, M. Muccini, R. Zamboni, F. Rossi, *Naturally functionalized silk as useful material for photonic applications,* JCOMB 2015, 71, 152-8.

87. C. Dionigi, T. Posati, V. Benfenati, A. Sagnella, S. Bonetti, G. Ruani, F. Dinelli, G. Padeletti, R. Zamboni, M. Muccini, *A nanostructured conductive bio-composite of silk fibroin–single walled carbon nanotubes,* J Mater Chem B 2014, 2, 1424-31.

88. L. Cappellozza, S. Cappellozza, A. Saviane, G. Sbrenna, *Artificial diet rearing system for the silkworm Bombyx mori (Lepidoptera: Bombycidae): effect of vitamin C deprivation on larval growth and cocoon production*, Appl Entomol Zool 2005, 40, 405-12.

89. S. Cappellozza, A. Saviane, *La dieta artificiale per il baco da seta: metodica per l'allevamento su piccola scala*, Apoidea 2009, 6, 45-56.

90. B. B. Mandal, S. C. Kundu, *A novel method for dissolution and stabilization of non-mulberry silk gland protein fibroin using anionic surfactant sodium dodecyl sulfate*, Biotechnol Bioeng 2008, 99, 1482-89.

91. C. Dionigi, M. Bianchi, P. D'Angelo, B. Chelli, P. Greco, A. Shehu, I. Tonazzini, A. Nicoleta Lazar, F. Biscarini, *Control of neuronal cell adhesion on single-walled carbon nanotube 3D patterns*, J Mater Chem 2010, 20, 2213-18.

92. C. Dionigi, P. Stoliar, G. Ruani, S. D. Quiroga, M. Facchini, F. Biscarini, *Carbon nanotube carriers for fabrication of ordered SWCNT networks*, J Mater Chem 2007, 17, 3681-86.

93. C. Dionigi, P. Nozar, D. Di Domenico, G. Calestani, *A simple geometrical model for emulsifier free polymer colloids formation,* J Colloid Interface Sci 2004, 275, 445-9.

94. N. C. Tansil, Y. Li, C. P. Teng, S. Zhang, K. Y. Win, X. Chen, X. Y. Liu and M.-Y. Han, *Intrinsically colored and luminescent silk*, Adv Mater 2011, 23, 1463-66.

95. N. C. Tansil, L. D. Koh, M.-Y. Han, *Functional silk: colored and luminescent,* Adv Mater 2011, 24, 1388-97.

96. G. Barbarella, M. Zambianchi, A. Ventola, E. Fabiano, F. Della Sala, G. Gigli, M. Anni, A. Bolognesi, L. Polito, M. Naldi, M. Capobianco, *Bright oligothiophene N-succinimidyl esters for efficient fluorescent labeling of proteins and oligonucleotides*, Bioconjugate Chem 2006, 17, 58-67.

97. M. K. Sah, K. Pramanik, *Regenerated silk fibroin from B. mori silk cocoon for tissue engineering applications,* IJESD 2010, 1,404–8.

98. L. S. Wray, X. Hu, J. Gallego, I. Georgakoudi, F. G. Omenetto, D. Schmidt, D. L. Kaplan, *Effect of processing on silk-based biomaterials: Reproducibility and biocompatibility*, J Biomed Mater Res B Appl Biomater 2011, 99, 89-101.

99. H. Yamada, H. Nakao, Y. Takasua, K. Tsubouchi, *Preparation of undegraded native molecular fibroin solution from silkworm cocoons,* Mater Sci Eng C 2001, 14, 41-6.

100. T. Asakura, Y. Watanabe, A. Uchida, H. Minagawa, *NMR of Silk Fibroin, ^{13}C NMR study of the chain dynamics and solution structure of Bombyx mori silk fibroin,* Macromolecules 1984, 17, 1075–81.

101. Zainuddin, T. T. Le, Y. Park, T. V. Chirila, P. J. Halley, A. K. Whittaker, *The behavior of aged regenerated Bombyx mori silk fibroin solutions studied by ^{1}H NMR and rheology*, Biomaterials 2008, 29, 4268–74.

102. X. Hu, D. L. Kaplan, P. Cebe, *Determining beta-sheet crystallinity in fibrous proteins by thermal analysis and infrared spectroscopy,* Macromolecules 2006, 39, 6161–70.

103. P. Monti, P. Taddei, G. Freddi, T. Asakura, M. Tsukada, *Raman spectroscopic characterization of Bombyx mori silk fibroin: Raman spectrum of Silk I*, J Raman Spectrosc 2001, 32, 103–7.

104. K. Nagayama, *Two-dimensional self-assembly of colloids in thin liquid films*, Colloids Surfaces A 1996, 109, 363-74.

105. A. S. Dimitrov, K. Nagayama, *Steady-state unidirectional convective assembling of fine particles into two-dimensional arrays,* Chem Phys Lett 1995, 243, 462-68.

106. X. Hu, D. L Kaplan, P. Cebe, *Dynamic protein-water relationships during β-sheet formation*, Macromolecules 2008, 41, 3939-48.

107. Q. Lu, X. Hu, X. Wang, J. A. Kluge, S. Lu, P. Cebe, D. L. Kaplan, *Water-Insoluble Silk Films with Silk I Structure,* Acta Biomater 2010, 1380–7.

108. A. Motta, L. Fambri, C. Migliaresi, *Regenerated silk fibroin films: Thermal and dynamic mechanical analysis*, Macromol Chem Phys 2002, 203, 1658-65.

109. Q. Lu, B. Zhang, M. Li, B. Zuo, D. L. Kaplan, Y. Huang, H. Zhu, *Degradation mechanism and control of silk fibroin*, Biomacromolecules 2011, 12, 1080-6.

110. K. Yamada, Y. Tsuboi, A. Itaya, *AFM observation of silk fibroin on mica substrates: morphologies reflecting the secondary structures,* Thin Solid Films 2003, 440, 208–16.

111. E. Servoli, D. Maniglio, A. Motta, R. Predazzer, C. Migliaresi, *Surface properties of silk fibroin films and their interaction with fibroblasts,* Macromol Biosci 2005, 5, 1175–83.

112. M. Darder, P. Aranda, E. Ruiz-Hitzky, *Bionanocomposites: a new concept of ecological, bioinspired, and functional hybrid materials*, Adv Mater 2007, 19, 1309−19.

113. E. Ruiz-Hitzky, M. Darder, P. Aranda, K. Ariga, *Advances in biomimetic and nanostructured biohybrid materials*, Adv Mater 2010, 22, 323−36.

114. N. Bitinis, M. Hernandez, R. Verdejo, J. M. Kenny, M. A. Lopez-Manchado, *Recent advances in clay/polymer nanocomposites*, Adv Mater 2011, 23, 5229−36.

115. E. Kharlampieva, V. Kozlovskaya, B. Wallet, V. V. Shevchenko, R. R. Naik, R. Vaia, D. L. Kaplan, V. V. Tsukruk, *Co-cross-linking silk matrices with silica nanostructures for robust ultrathin nanocomposites*, Nano 2010, 4, 7053−63.

116. E. Kharlampieva, V. Kozlovskaya, R. Gunawidjaja, V. V. Shevchenko, R. R. Naik, R. Vaia, D. L. Kaplan, V. V. Tsukruk, *Flexible silk–inorganic nanocomposites: from transparent to highly reflective*, Adv Funct Mater 2010, 20, 840−6.

117. V. Rives, *Layered Double Hydroxides: Present and Future*; Nova Science Publishers: New York, 2001.

118. J. H. Choy,S. Y. Kwak, Y. J. Jeong, J. S. Park, *Innovative layered double hydroxides as non viral vectors*, Angew Chem, Int Ed 2000, 39, 4042−5.

119. V. Ambrogi, V. Ciarnelli, M. Nocchetti, L. Perioli, C. Rossi, Effect of hydrotalcite-like compounds on the aqueous solubility of some poorly water-soluble drugs, Eur J Pharm Sci 2009, 73, 285−91.

120. T. Posati, F. Bellezza, A. Cipiciani, F. Costantino, M. Nocchetti, L. Tarpani, L Latterini, *Synthesis and characterization of luminescent nanoclays,* Cryst Growth Des 2010, 10, 2847−50.

121. J. T. Kloprogge, L. Hickey, R. L. Frost, *The effects of synthesis pH and hydrothermal treatment on the formation of zinc aluminum hydrotalcites*, Solid State Chem 2004, 177, 4047−57.

122. C. S. Chen, S. Soni, C. Le, M. Biasca, E. Farr, E. Y. Chen, W. C. Chin, *Human stem cell neuronal differentiation on silk-carbon nanotube composite*, Nanoscale Res Lett 2012, 7, 126-33.

123. G. A. Silva, *Neuroscience nanotechnology: progress, opportunities and challenges.*, Nat Rev Neurosci, 2006, 7, 65-74.

124. P. Zorlutuna, N. Annabi, G. Camci-Unal, M. Nikkhah, J. M. Cha, J. W. Nichol, A. Manbachi, H. Bae, S. Chen, A. Khademhosseini, *Microfabricated biomaterials for engineering 3D tissues,* Adv Mater 2012, 24, 1782-1804.

125. E. B. Malarkey, A. Fisher, E. Bekyarova, W. Liu, R. C. Haddon, V. Parpura, *Conductive single-walled carbon nanotube substrates modulate neuronal growth,* Nano Lett 2009, 9, 264-8.

126. D. H. Kim, J. Viventi, J. J. Amsden, J. Xiao, L. Vigeland, Y. S. Kim, J. A. Blanco, B. Panilaitis, E. S. Frechette, D. Contreras, D. L. Kaplan, F. G. Omenetto, Y. Huang, K. C. Hwang, M. R. Zakin, B. Litt and J. A. Rogers, *Dissolvable films of silk fibroin for ultrathin conformal bio-integrated electronics*, Nat Mater 2010, 9, 511-7.

127. P. T. C. So, C. Y. Dong, B. R. Masters, K. M. Berland, *Two-photon excitation fluorescence microscopy*, Annu Rev Biomed Eng 2000, 02, 399-429.

128. Y. Yang, Z. Shao, X. Chen, P. Zhou, *Optical spectroscopy to investigate the structure of regenerated Bombyx mori silk fibroin in solution*, Biomacromolecules 2004, 5, 773-9.

129. I. Georgakoudi, I. Tsai, C. Greiner, C. Wong, J. De Felice, D. L. Kaplan, *Intrinsic fluorescence changes associated with the conformational state of silk fibroin in biomaterial matrices,* OSA 2007, 15, 1043-53.

130. Y. K. Reshetnyak, Y. Koshevnik, E. A. Burstein, *Decomposition of protein tryptophan fluorescence spectra into log-normal components. III. Correlation between fluorescence and microenvironment parameters of individual tryptophan residues*, Biophys J 2001, 81, 1735-58.

131. D. A. Malencik and S. R. Anderson, *Dityrosine as a product of oxidative stress and fluorescent probe,* Amino Acids 2003, 25, 233-47.

132. H. Zhao, E. Heusler, G. Jones, L. Li, V. Werner, O. Germershaus, J. Ritzer, T. Luehmann, L. Meinel, *Decoration of silk fibroin by click chemistry for biomedical application*, J Struct Biol 2014, 186, 420-30.

133. R. G. Acres, A. V. Ellis, J. Alvino, C. E. Lenahan, D. A. Khodakov, G. F. Metha, G. G. Andersson, *Molecular Structure of 3-Aminopropyltriethoxysilane Layers Formed on Silanol-Terminated Silicon Surfaces*, J Phys Chem C 2012, 116, 6289-97.

134. M. Melucci, M. Zambianchi, L. Favaretto, V. Palermo, E. Treossi, M. Montalti, S. Bonacchi, M. Cavallini, *Multicolor, large-area fluorescence sensing through oligothiophene-self-assembled monolayers,* Chem Commun 2011, 47, 1689-91.

135. Y. Cohen, L. Avram, L. Frich, *Diffusion NMR spectroscopy in supramolecular and combinatorial chemistry: an old parameter—new insights,* Angew Chem Int Ed 2005, 4, 520-54.